
Latent Optimal Paths by Gumbel Propagation for Variational Bayesian Dynamic Programming

Xinlei Niu¹ Christian Walder² Jing Zhang¹ Charles Patrick Martin¹

Abstract

We propose the stochastic optimal path which solves the classical optimal path problem by a probability-softening solution. This unified approach transforms a wide range of DP problems into directed acyclic graphs in which all paths follow a Gibbs distribution. We show the equivalence of the Gibbs distribution to a message-passing algorithm by the properties of the Gumbel distribution and give all the ingredients required for variational Bayesian inference of a latent path, namely Bayesian dynamic programming (BDP). We demonstrate the usage of BDP in the latent space of variational autoencoders (VAEs) and propose the BDP-VAE which captures structured sparse optimal paths as latent variables. This enables end-to-end training for generative tasks in which models rely on unobserved structural information. At last, we validate the behaviour of our approach and showcase its applicability in two real-world applications: text-to-speech and singing voice synthesis. Our implementation code is available at <https://github.com/XinleiNIU/LatentOptimalPathsBayesianDP>.

1. Introduction

Optimal paths are often required in many generative tasks such as speech, music, and language modeling (Kim et al., 2020; Li et al., 2022; Cai et al., 2019). These tasks involve the simultaneous identification of structured relationships between data and conditions. Obtaining optimal paths given a graph constraint with weights to achieve an improved fit based on extracted unobserved structural features. In the context of optimal path problems, such as finding the short-

est path in a graph, dynamic programming (DP) efficiently computes the solution by breaking the problem down into several sub-problems and finding optimal solutions within the sub-problems iteratively.

Since the DP algorithm finds shortest paths using the max operator, it is non-differentiable which limits the usage of optimal paths in neural networks where gradient back-propagation is applied. As a workaround, previous works have approximated the max operator with smoothed functions to allow differentiation of DP algorithms (Verdu & Poor, 1987). However, smoothed approximations lose the sparsity of solutions which makes hard assignments become soft assignments. Alternatively, some real-world generative applications (Ren et al., 2019; 2020; Jeong et al., 2021; Li et al., 2022; Halperin et al., 2019; Peng et al., 2020; Liu et al., 2022; Popov et al., 2021), that require to integrate structured optimal paths, split the training strategies in which neural network models depend on sparse outputs from external DP aligners (McAuliffe et al., 2017; Hasegawa-Johnson et al., 2005) or pre-trained models (Li et al., 2018). However, these external components involve more than one training phase thus the model performance critically relies on them.

In this work, we explore a novel and unified method to obtain structured sparse optimal paths in the latent space of variational autoencoders (VAEs) with DP. Instead of a smoothed approximation for the classical optimal path problem, we propose the stochastic optimal path, which is a probabilistic softening solution by defining a Gibbs distribution where the energy function is the path score. We show this to be equivalent to a message-passing algorithm on the directed acyclic graphs (DAG) using the max and shift properties of the Gumbel distribution. To learn the latent optimal paths, we give tractable ingredients for variational Bayesian inference (i.e., likelihood and KL divergence) using DP, namely Bayesian dynamic programming (BDP), as well as an efficient sampling algorithm, which enables VAEs to obtain latent optimal paths within a DAG and achieve end-to-end training on generative tasks that rely on sparse unobserved structural relationships. We make the following contributions:

- (1) We present a unified framework that gives a probabilistic softening of the classical optimal path problem on DAGs.

¹Australian National University, Canberra, Australia ²Google, DeepMind, Montreal, Canada. Correspondence to: Xinlei Niu <xinlei.niu@anu.edu.au>.

We notably give efficient algorithms in linear time for sampling, computing the likelihood, and computing the KL divergence, thereby providing all of the ingredients required for variational Bayesian inference with a latent optimal path.

(2) We introduce BDP-VAE that learns sparse latent optimal paths. In the case of conditional generation, the data is not observed during inference, it is difficult to form the distribution statistics (i.e., edge weights) in the prior encoder. We give an alternative and flexible method to form the distribution statistics on the conditional prior by making use of a flow-based model.

(3) We demonstrate how the BDP-VAE achieves end-to-end training on two real-world challenging applications (i.e., text-to-speech (TTS) and singing voice synthesis (SVS)) and verify the behaviour of the stochastic optimal paths, latent paths and hyper-parameters proposed in Section 4 and Section 5.

2. Related Work

Since traditional DP finding optimal paths is non-differentiable, there exist many alternative works that integrate DP into the neural networks by involving a convex optimization problem (Amos & Kolter, 2017; Djolonga & Krause, 2017). Instead, Mensch & Blondel (2018) proposed a unified DP framework by turning a broad class of DP problems into a DAG and obtaining the optimal path by a max operator smoothed with a strongly convex regularizer. This work can be applied in structured prediction tasks (BakIr et al., 2007) under supervised learning. Inspired by Mensch & Blondel (2018), we proposed a probabilistic softening solution to seek stochastic optimal paths with a path distribution under a DAG. Graphical models such as Bayesian networks (Heckerman, 1998) learn dependencies of random variables based on a DAG, our method treats the paths of a DAG, not the nodes, as random variables of a Gibbs distribution.

In many conditional generative tasks, models usually rely on structured dependencies of data and conditions, in which the dependencies are unobserved. Ren et al. (2020) and Liu et al. (2022) use a multiple training strategy by obtaining the sparse dependencies from an external DP-based techniques (McAuliffe et al., 2017) at first, then use the outputs as additional inputs to the model. Kim et al. (2020) integrates a DP on a Glow-based model to obtain unobserved monotonic alignment in parallel. Other models with structured latent representations such as HMMs (Rabiner, 1989) and PCFGs (Petrov & Klein, 2007) make strong assumptions about the model structure which could limit their flexibility and applicability. Instead of these works, we propose a unified framework to enable the VAEs (Kingma & Welling, 2014) to capture structural latent variables (i.e.,

sparse optimal paths), allowing for flexible adaptation to a variety of downstream tasks.

The attention mechanism is widely applied for obtaining unobserved dependencies in many seq-to-seq tasks. Deng et al. (2018) makes use of the properties of VAEs and captures the unobserved non-structural dependencies by learning latent alignment with attention in VAEs. However, to obtain structural constraints, attention strongly relies on model structures and other techniques such as DP to extract marginalization of the attention alignment distribution (Yu et al., 2016b;a). Different from latent alignment with attention, we target solving the optimal path problem in a unified framework that can be easily adapted to any structural constraint by defining DAGs. By capturing unobserved sparse shortest paths under the defined DAG in a latent space, our BDP-VAE facilitates the development of more explicit structural unobserved dependencies for a variety of applications. Secondly, attention mechanisms can be computationally expensive, especially for large input sequences. Solutions such as Chiu & Raffel (2018) reduce the computational complexity by involving a DP. Our method seeks stochastic optimal paths that occur in linear time with respect to edge numbers of DAGs (Corollary 4.11).

The Gumbel-Max trick makes use of the max property of the Gumbel distribution which allows for efficient sampling from discrete distributions (Maddison et al., 2014). Jang et al. (2017) and Maddison et al. (2017) facilitate gradient-based learning for Gibbs distribution by relaxing the component-wise optimization in the Gumbel-Max trick. Struminsky et al. (2021) focuses on leveraging the Gumbel-Max trick on the score function estimator. Unlike those, our research leverages the max and shift properties of Gumbel distribution for message-passing on DP to obtain ingredients required for variational Bayesian inference for latent paths.

3. Preliminaries

This section provides background on the notation definition of a DAG, a definition of the traditional optimal path problem given a DAG, and properties of the Gumbel random variable.

Definition of a Graph: We denote $\mathcal{R} = (\mathcal{V}, \mathcal{E})$ be a directed acyclic graph with nodes \mathcal{V} and edges \mathcal{E} . Assume without loss of generality that the nodes are numbered in topological order, such that $\mathcal{V} = (1, 2, \dots, N)$ and $u < v$ for all $(u, v) \in \mathcal{E}$. Further, we assume that 1 is the only node without parents and N the only node without children. We denote the edge weights $\mathbf{W} \in \mathbb{R}^{N \times N}$ with $w_{i,j} = -\infty$ for all $(u, v) \notin \mathcal{E}$. Let $\mathcal{Y}(1, v)$ be the set of all paths from 1 to v . Associate with each path $\mathbf{y} = (y_1, y_2, \dots, y_{|\mathbf{y}|})$ a score obtained by summing edge weights along the path, defined as $\|\mathbf{y}\|_{\mathbf{W}} = \sum_{i=2}^{|\mathbf{y}|} w_{y_{i-1}, y_i} = \sum_{(u,v) \in \mathbf{y}} w_{u,v}$, where

the final expression introduces the notation $(u, v) \in \mathbf{y}$ for the edges (u, v) that make up path \mathbf{y} . Denote the set of parents of node v by $\mathcal{P}(v) = \{u : (u, v) \in \mathcal{E}\}$ and the set of children of node u by $\mathcal{C}(u) = \{v : (u, v) \in \mathcal{E}\}$.

Non-Stochastic Optimal Paths: The traditional optimal path problem is to find the highest scoring path from node 1 to node N ,

$$\mathbf{y}^* = \operatorname{argmax}_{\mathbf{y} \in \mathcal{Y}(1, N)} \|\mathbf{y}\|_{\mathbf{W}}. \quad (1)$$

This can be solved in $O(|\mathcal{E}|)$ time by iterating in topological order. The score $\xi(\cdot)$ is defined as

$$\xi(1) = 0 \quad (2)$$

$$\forall v \in \{2, 3, \dots, N\}, \quad \xi(v) = \max_{u \in \mathcal{P}(v)} \xi(u) + w_{u,v}, \quad (3)$$

after which \mathbf{y}^* is obtained (in reverse) by tracing from N to 1, following the path of nodes u for which the maximum was obtained in the above.

Gumbel Random Variable: Let $\mathcal{G}(\mu)$ denote the unit scale Gumbel random variable with location parameter μ and probability density function

$$\mathcal{G}(x|\mu) = \exp(-(x - \mu) - \exp(x - \mu)). \quad (4)$$

We now review the properties of the Gumbel which we will exploit in Section 4. Let $X \sim \mathcal{G}(\mu)$. The Gumbel distribution is closed under shifting, with

$$X + \text{const.} \sim \mathcal{G}(\mu + \text{const.}). \quad (5)$$

Let $X_i \sim \mathcal{G}(\mu_i)$ for all $i \in \{1, 2, \dots, m\}$. The Gumbel is also closed under the max operation, with

$$\max(\{X_1, X_2, \dots, X_m\}) \sim \mathcal{G}(\log \sum_{i=1}^m \exp(\mu_i)). \quad (6)$$

Finally, there is a closed-form expression for the index which obtains the maximum in the above expression:

$$p(k = \operatorname{argmax}_{i \in \{1, 2, \dots, m\}} X_i) = \frac{\exp(\mu_k)}{\sum_{i=1}^m \exp(\mu_i)}. \quad (7)$$

4. Bayesian Dynamic Programming

In this section, we propose a stochastic approach to seek optimal paths. We denote a distribution family given a DAG with edge weights and give ingredients required for variational Bayesian inference by using DP with Gumbel propagation, namely, Bayesian dynamic programming.

4.1. Stochastic Optimal Paths

In the stochastic approach, every possible path $\mathbf{y} \in \mathcal{Y}$ on \mathbf{W} follows a Gibbs distribution given a DAG \mathcal{R} , edge weights \mathbf{W} and temperature parameter α defined by Definition 4.1.

Definition 4.1. Denote by

$$\mathcal{D}(\mathcal{R}, \mathbf{W}, \alpha) \quad (8)$$

the Gibbs distribution over $\mathbf{y} \in \mathcal{Y}(1, N)$ with probability mass function

$$\mathcal{D}(\mathbf{y}|\mathcal{R}, \mathbf{W}, \alpha) = \frac{\exp(\alpha \|\mathbf{y}\|_{\mathbf{W}})}{\sum_{\hat{\mathbf{y}} \in \mathcal{Y}(1, N)} \exp(\alpha \|\hat{\mathbf{y}}\|_{\mathbf{W}})}. \quad (9)$$

Despite the intractable form of the denominator in Equation (9), we provide the ingredients necessary for approximate Bayesian inference for latent distribution (unobserved) \mathcal{D} . In particular, we can efficiently compute the normalized likelihood (Corollary 4.6), sample (Corollary 4.7), and compute the KL divergence within $\mathcal{D}(\mathcal{R}, \cdot, \alpha)$ (Lemma 4.10) in linear time (Corollary 4.11).

4.2. Gumbel Propagation

The Gumbel propagation offers an equivalent formulation of Definition 4.1 that lends itself to dynamic programming by the properties in Equation (7) and Equation (5) as per the following result. Proofs per lemma of this subsection are in Appendix A.

Lemma 4.2. *Let*

$$Y = \operatorname{argmax}_{\mathbf{y} \in \mathcal{Y}(1, N)} \{\Omega_{\mathbf{y}}\}, \quad (10)$$

where for all $\mathbf{y} \in \mathcal{Y}(1, N)$,

$$\Omega_{\mathbf{y}} = \alpha \|\mathbf{y}\|_{\mathbf{W}} + G_{\mathbf{y}} \quad (11)$$

$$G_{\mathbf{y}} \sim \mathcal{G}(0). \quad (12)$$

Then the probability of $Y = \mathbf{y}$ is given by (9).

Let the definitions of $\Omega_{\mathbf{y}}$ and $G_{\mathbf{y}}$ extend to all $\mathbf{y} \in \bigcup_{u=1}^N \mathcal{Y}(1, u)$, which is the set of all partial paths. We define for each node $v \in \mathcal{V}$ the real-valued random variable

$$Q_v = \max_{\mathbf{y} \in \mathcal{Y}(1, v)} \{\Omega_{\mathbf{y}}\}. \quad (13)$$

Therefore, Q_v allows us to set up a recursion on the entire DAG \mathcal{R} .

Lemma 4.3. *The Q_v are Gumbel distributed with*

$$Q_v \sim \mathcal{G}(\mu_v), \quad (14)$$

where

$$\mu_v = \log \sum_{\mathbf{y} \in \mathcal{Y}(1, v)} \exp(\alpha \|\mathbf{y}\|_{\mathbf{W}}). \quad (15)$$

We now state the first main result in Lemma 4.4.

Lemma 4.4. *The location parameters μ_v satisfy the recursion*

$$\mu_1 = 0 \quad (16)$$

$$\mu_v = \log \sum_{u \in \mathcal{P}(v)} \exp(\mu_u + \alpha w_{u,v}). \quad (17)$$

for all $v \in \{2, 3, \dots, N\}$.

4.3. Sampling and Likelihood

Then we state an alternative normalized likelihood of a sampled path \mathbf{y} by Corollary 4.7 as Corollary 4.6 according to a transition matrix defined in Lemma 4.5. The transition matrix in Lemma 4.5 can be computed according to the location parameter μ defined in Lemma 4.4 directly. Proofs per lemma of this subsection are in Appendix B.

Lemma 4.5. *Let paths $\mathbf{y} = (y_1, y_2, \dots, y_{|\mathbf{y}|})$ denotes the component of the random variable Y defined in (10), given that $Y = (y_1, y_2, \dots, y_{|\mathbf{y}|})$. The probability of the transition $v \rightarrow u$ is*

$$\pi_{u,v} \equiv p(y_{i-1} = u | y_i = v, u \in \mathcal{P}(v)) \quad (18)$$

$$= \frac{\exp(\mu_u + \alpha w_{u,v})}{\exp(\mu_v)}, \quad (19)$$

for all $i \in \{2, 3, \dots, N\}$.

Corollary 4.6. *The path probability may be written*

$$\mathcal{D}(\mathbf{y} | \mathcal{R}, \mathbf{W}, \alpha) = \prod_{(u,v) \in \mathbf{y}} \pi_{u,v}. \quad (20)$$

Corollary 4.7. *Paths $\mathbf{y} \sim \mathcal{D}(\mathcal{R}, \mathbf{W}, \alpha)$ may be sampled (in reverse) by*

1. Initialising $v = N$,
2. sampling $u \in \mathcal{P}(v)$ with probability $\pi_{u,v}$,
3. setting $v \leftarrow u$,
4. if $v = 1$ then stop, otherwise return to step 2.

4.4. KL Divergence

Given $\mathcal{D}(\mathcal{R}, \mathbf{W}, \alpha)$ and $\mathcal{D}(\mathcal{R}, \mathbf{W}^{(r)}, \alpha)$, where $\mathbf{W}^{(r)}$ are edge weights have different values to \mathbf{W} . We give a tractable closed-form of the KL divergence within the distribution family of $\mathcal{D}(\mathcal{R}, \cdot, \alpha)$ in Lemma 4.10. Proofs per lemma of this subsection are in Appendix C.

Definition 4.8. We denote the total probability of paths that include a given edge $(u, v) \in \mathcal{E}$ by

$$\omega_{u,v} \equiv \sum_{\{\mathbf{y} \in \mathcal{Y}(1,N) : (u,v) \in \mathbf{y}\}} \mathcal{D}(\mathbf{y} | \mathcal{R}, \mathbf{W}, \alpha). \quad (21)$$

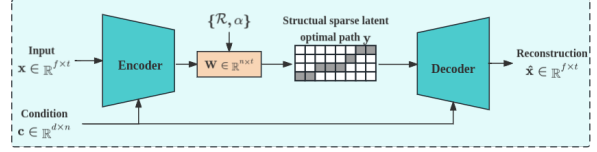


Figure 1: A pipeline of BDP-VAE, BDP-VAE captures the unobserved sparse structural dependency (i.e., optimal paths) in the latent space in parallel training the model and allows gradient-based optimization for learning the edge weights \mathbf{W} .

The quantity in the above definition may be computed using two dynamic programming passes, one topologically ordered and the other reverse topologically ordered, by applying the following

Lemma 4.9. *For all $(u, v) \in \mathcal{E}$,*

$$\omega_{u,v} = \pi_{u,v} \lambda_u \rho_v, \quad (22)$$

where we have the recursions

$$\lambda_1 = 1 \quad (23)$$

$$\lambda_v = \sum_{u \in \mathcal{P}(v)} \lambda_u \pi_{u,v} \quad (24)$$

for all $v \in \{2, 3, \dots, N\}$ (in topological order w.r.t. \mathcal{R}), and

$$\rho_N = 1 \quad (25)$$

$$\rho_u = \sum_{v \in \mathcal{C}(u)} \rho_v \pi_{u,v} \quad (26)$$

for all $u \in \{N-1, N-2, \dots, 1\}$ (in reverse topological order w.r.t. \mathcal{R}).

Lemma 4.10. *The KL divergence within the family $\mathcal{D}(\mathcal{R}, \cdot, \alpha)$ is*

$$\begin{aligned} \mathcal{D}_{\text{KL}} \left[\mathcal{D}(\mathcal{R}, \mathbf{W}, \alpha) \parallel \mathcal{D}(\mathcal{R}, \mathbf{W}^{(r)}, \alpha) \right] \\ = \mu_N^{(r)} - \mu_N + \alpha \sum_{(u,v) \in \mathcal{E}} \omega_{u,v} (w_{u,v} - w_{u,v}^{(r)}), \end{aligned} \quad (27)$$

where $\omega_{u,v}$ is the marginal probability of edge (u, v) on $\mathcal{D}(\mathcal{R}, \mathbf{W}, \alpha)$ defined in Definition 4.8, μ_N is defined in Equation (15) and $\mu_N^{(r)}$ is similar to μ_N but defined in terms of $\mathbf{W}^{(r)}$ rather than \mathbf{W} .

Corollary 4.11. *The KL divergence (27), the likelihood (20), and the sampling algorithm (Corollary 4.7) may be computed in $O(|\mathcal{E}|)$ time.*

5. BDP-VAE

We now show how to apply the method in Section 4 to a conditional VAE framework to obtain sparse latent optimal paths. An unconditional BDP-VAE framework can be directly applied based on Corollary 4.6, Corollary 4.7, and Lemma 4.10, but a conditional BDP-VAE framework may be challenging in real applications. Given a sequential-like input \mathbf{x} with length t and a sequential-like condition \mathbf{c} with length n , where $t \neq n$ and $\{t, n\}$ are varying within the dataset. We wish to find an unobserved hard structural relationship between \mathbf{x} and \mathbf{c} in the latent space of VAEs denoted as \mathbf{y} . Conditional BDP-VAEs consist of three parts: an encoder models posterior distribution $q(\mathbf{y}|\mathbf{x}, \mathbf{c}; \phi)$, a decoder models the distribution of $p(\mathbf{x}|\mathbf{y}, \mathbf{c}; \theta)$, and a prior encoder models the prior distribution $p(\mathbf{y}|\mathbf{c}; \theta)$. An overview pipeline of BDP-VAE is in Figure 1, which captures structured sparse optimal paths in the latent space.

We assume the conditional input \mathbf{c} is always observed and the conditional ELBO is defined as

$$\mathcal{L}(\phi, \theta, \mathbf{x}|\mathbf{c}) = \mathbb{E}_{\mathbf{y} \sim q(\cdot|\mathbf{x}, \mathbf{c}; \phi)} [\log p(\mathbf{x}|\mathbf{y}, \mathbf{c}; \theta)] - \mathcal{D}_{\text{KL}} [q(\mathbf{y}|\mathbf{x}, \mathbf{c}; \phi) \| p(\mathbf{y}|\mathbf{c}; \theta)]. \quad (28)$$

5.1. Posterior and Latent Optimal Paths

Given a DAG \mathcal{R} with edge \mathcal{E} and nodes \mathcal{V} , the distribution of the posterior encoder is denoted as

$$q(\mathbf{y}|\mathbf{x}, \mathbf{c}; \phi) = \mathcal{D}(\mathbf{y}|\mathcal{R}, \mathbf{W} = \text{NN}_{\mathbf{W}}(\mathbf{x}, \mathbf{c}; \phi), \alpha) \quad (29)$$

where $\text{NN}_{\mathbf{W}}(\cdot; \phi)$ is a neural network to learn the edge weights \mathbf{W} of the DAG \mathcal{R} and α is a hyper-parameter. The latent optimal path \mathbf{y} with $\{0, 1\}$ can be sampled reversely according to Lemma 4.5 and Corollary 4.7. As a result, \mathbf{y} forms a *sparse matrix* with dimensions identical to those of the weight matrix \mathbf{W} . As shown in Figure 1, the sparsity and structure of \mathbf{y} are inherently achieved through its construction using the DAG \mathcal{R} ¹.

5.2. Conditional Prior

Denote the distribution of the conditional prior as

$$p(\mathbf{y}|\mathbf{c}; \theta) = \mathcal{D}(\mathbf{y}|\mathcal{R}, \mathbf{W}^{(0)} = \text{NN}_{\mathbf{W}^{(0)}}(\mathbf{c}; \theta), \alpha) \quad (30)$$

We have provided a closed-form KL divergence within the family $\mathcal{D}(\mathcal{R}, \cdot, \alpha)$ in Lemma 4.10 which may be convenient for unconditional generation by pre-setting the prior distribution statistics directly. In most conditional generation

¹In the case where the structure of DAGs \mathcal{R} is unknown. Since we are learning the DAG weights \mathbf{W} and zero weights are equivalent to removing an edge, in some sense the BDP algorithm can in principle learn an approximate DAG structure by imposing small edge weight values. However, in this study, we target to verify our method on applications with a clear prior knowledge of structure DAGs.

tasks, the non-accessible \mathbf{x} during the inference phase in real applications leads to problems on the prior encoder when forming the edge weights $\mathbf{W}^{(0)}$ given information of \mathbf{c} only, especially in the case that \mathbf{x} has varying lengths t . To address this issue, we give a flexible solution for inferring feature information of \mathbf{x} given \mathbf{c} to form the edge weights $\mathbf{W}^{(0)}$ in the conditional prior. Inspired by Ma et al. (2019), we make use of a flow-based model to infer information of \mathbf{x} condition on \mathbf{c} and further form the $\mathbf{W}^{(0)}$. Assume there exists a series of invertible transformations random variables \mathbf{x} , such that

$$\mathbf{x} \xleftarrow[g_1]{f_1} \cdots \xleftarrow[g_k]{f_k} \mathbf{c} \xleftarrow[g_{k+1}]{f_{k+1}} \cdots \xleftarrow[g_K]{f_K} v \quad (31)$$

where $f = f_1 \circ \cdots \circ f_K$ and $v \sim N(0, 1)$ (θ is omitted for brevity), the KL divergence term in Equation (28) can be written as

$$\mathcal{D}_{\text{KL}} [q(\mathbf{y}|\mathbf{x}, \mathbf{c}; \phi) \| p(\mathbf{y}|\mathbf{c}; \theta)] \quad (32)$$

$$= \mathcal{D}_{\text{KL}} [q(\mathbf{y}|\mathbf{x}, \mathbf{c}; \phi) \| p(\mathbf{y}|\mathbf{x}, \mathbf{c}; \theta)] - \log p(\mathbf{x}|\mathbf{c}; \theta) \\ = -\log p_{N(0,1)}(f_{\theta}(\mathbf{x})) \left| \det \left(\frac{\partial f_{\theta}(\mathbf{x})}{\partial \mathbf{x}} \right) \right| \quad (33)$$

The backward pass is to infer the KL divergence during training. The forward pass is to infer feature information of \mathbf{x} given \mathbf{c} and form edge weight $\mathbf{W}^{(0)}$ during inference.

5.3. Learning

Based on the idea of Mohamed et al. (2020), the gradient of the ELBO (28) with respect to θ is straightforward, however, the gradient with respect to ϕ of the reconstruction error part in the ELBO is non-trivial. We make use of the REINFORCE estimator

$$\nabla_{\phi} \mathbb{E}_{\mathbf{y} \sim q(\cdot|\mathbf{x}, \mathbf{c}; \phi)} [\log p(\mathbf{x}|\mathbf{y}, \mathbf{c}; \theta)] \\ = \log p(\mathbf{x}|\tilde{\mathbf{y}}, \mathbf{c}; \theta) \nabla_{\phi} \log q(\tilde{\mathbf{y}}|\mathbf{x}, \mathbf{c}; \phi), \quad (34)$$

where $\tilde{\mathbf{y}}$ is an exact sample via Corollary 4.7 from the posterior $q(\cdot|\mathbf{x}, \mathbf{c}; \phi)$, and we recall that $\log q(\tilde{\mathbf{y}}|\mathbf{x}, \mathbf{c}; \phi)$ may be computed using the efficient and exact closed-form of Equation (20), and automatically differentiated.

Alternatively, we provide hints of Gumbel softmax trick to avoid using the REINFORCE estimator in Appendix D for interested readers. In this study, we focus on evaluating the closed form of latent sparse optimal paths. Compared to the reparameterization trick discussed in Appendix D, the log-derivative method (i.e., the REINFORCE estimator) has the advantage of being the most straight-forward, is formally unbiased, does not require the temperature parameter, and allows fast evaluation with the closed form expression of sparse paths \mathbf{y} in Equation (20).

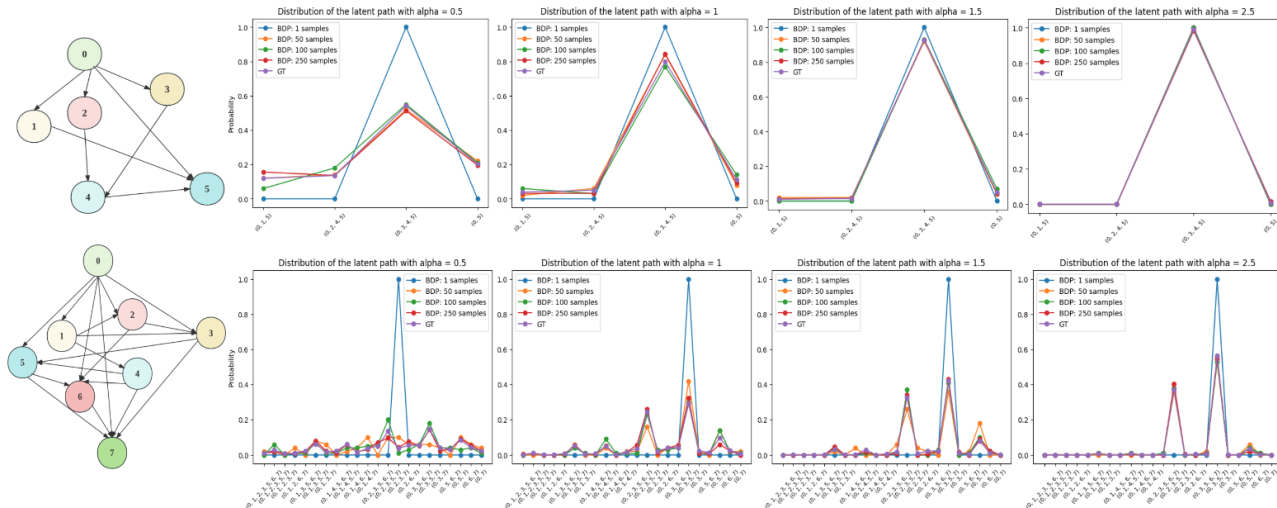


Figure 2: Toy experiments on BDP to find stochastic optimal paths. *The first row is a 5-node DAG and density plots with different α . The second row is an 8-node DAG and density plots with different α .*

6. Experiments

In this section, we conduct four experiments to verify our method from Section 4 and Section 5, and show its applicability on two real-world applications. To show the generalization of methods in Section 4, we extend BDP to two common application examples of computational graphs: monotonic alignment (MA) (Kim et al., 2020) and dynamic time warping (DTW) (Sakoe & Chiba, 1978; Mensch & Blondel, 2018). Details of examples of computational graphs, pseudo-codes, and time complexity analysis are provided in Appendix E. We provide detailed model architecture used in our experiments in Appendix F and experimental details and setup in Appendix G.

6.1. Stochastic Optimal Paths on Toy DAGs

We conduct an experiment to demonstrate how BDP in Section 4 finds the optimal paths on toy DAGs, in which the DAG structures and edge values are randomly generated. In Figure 2, we plot approximated density plots of path distributions with 1, 50, 100, and 250 samples by BDP compared with the corresponding ground truth path density plot. As BDP samples increase, the distribution of path samples will eventually converge to the real path distribution.

We then studied how the value of the temperature parameter α affects the path distribution. The larger α is, the sharper the distribution is, leading to an accurate optimal path result with less sample time. Conversely, for too small α , the BDP needs more samples to obtain the optimal path. We conduct another experiment to connect this finding with BDP-VAE in Section 6.5.

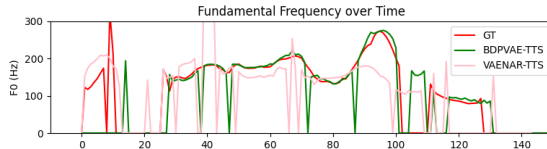


Figure 3: Inference F0 trajectory comparison with VAENAR-TTS of utterance "I suppose I have many thoughts.". *The intonation of BDPVAE-TTS is close to the GT indicating that sparse optimal paths help the decoder with a better understanding of how phoneme contributes to the overall utterance with approximated durations.*

6.2. Application: End-to-end Text-to-Speech

We apply the BDP-VAE framework with the computational graph of MA to perform an end-to-end TTS model on the RyanSpeech (Zandje et al., 2021) dataset. RyanSpeech contains 11279 audio clips (10 hours) of a professional male voice actor’s speech recorded at 44.1kHz. We randomly split 2000 clips for validation and 9297 clips for training.

The task of TTS involves an unobserved monotonic hard alignment that maps phonemes to time intervals since the order of the phonemes should be preserved while the duration of each may vary in speech. Thus, TTS models generate speech according to corresponding phonemes in which the duration of each phoneme is discrete, structural, and unobserved (Mehri et al., 2023). To show the BDP-VAE framework can be easily adapted into down-stream tasks, we redesign the popular non-end-to-end TTS model FastSpeech2 (Ren et al., 2020) into the BDP-VAE framework, namely BDPVAE-TTS, which can capture unobserved hard monotonic dependencies between phonemes and utterances jointly on both training and inference.

Table 1: Mel Cepstral Distortion (MCD) and Real-Time Factor (RTF) compared with other TTS models.

Model	Training	Align.(Train)	Align. (Infer)	MCD	RTF
FastSpeech2 (Ren et al., 2020) (Baseline)	Non end-to-end	Discrete	Continuous	9.96 ± 1.01	3.87×10^{-4}
Tacotron2 (Shen et al., 2018a)	End-to-end	Continuous	Continuous	11.39 ± 1.95	6.07×10^{-4}
VAENAR-TTS (Lu et al., 2021)	End-to-end	Continuous	Continuous	8.18 ± 0.87	1.10×10^{-4}
Glow-TTS (Kim et al., 2020)	End-to-end	Discrete	Continuous	8.58 ± 0.89	2.87×10^{-4}
BDPVAE-TTS (ours)	End-to-end	Discrete	Discrete	8.49 ± 0.96	3.00×10^{-4}

We verify model performance by an objective metric, the Mel cepstral distortion (MCD) (Kubichek, 1993; Chen et al., 2022), between ground truths and synthesized outputs. We record inference speed by real-time factor (RTF) per generated spectrogram frame. We randomly pick 70 sentences from the test set, the numerical results are shown in Table 1. Our method outperforms the baseline on both MCD and RTF and achieves end-to-end training. This shows the success of BDP-VAE in adapting a non-end-to-end model that relies on external DP aligners into an end-to-end pipeline.

We make a comparison with other end-to-end TTS models (Shen et al., 2018a; Kim et al., 2020; Lu et al., 2021) which target capturing phoneme dependencies. Shen et al. (2018a) models the unobserved temporal dependencies by an auto-regressive architecture with attention. Kim et al. (2020) integrate a monotonic alignment search in parallel in a Glow model (Kingma & Dhariwal, 2018) to obtain hard monotonic alignment. Lu et al. (2021) utilizes the latent Gaussian and captures soft monotonic alignment in the decoder by causality-masked self-attention. Among them, BDPVAE-TTS performs discrete alignment on both training and inference that ensures model consistency for training and inference. BDPVAE-TTS gets a better MCD and RTF than Shen et al. (2018a) and Kim et al. (2020), but gets higher MCD and RTF than Lu et al. (2021).

For the RTF, since BDPVAE-TTS involves a linear time consumption DP algorithm which causes higher inference time than VAENAR-TTS. We have discussed time complexity for each end-to-end TTS model in this experiment as below. However, the linear time consumption (Corollary 4.11) is the best we can do for solving a DP problem.

Time Complexity Analysis: Denote the maximum number of spectrogram frames in the computational graph of MA is T_{mel} and the maximum number of phoneme tokens in the computational graph of MA is T_{text} . In this experiment, BDPVAE-TTS obtains discrete latent monotonic paths by BDP with $\mathcal{O}(T_{mel})$ time complexity (detail implementations and discussion could be found in Appendix E.2.1). Besides, the time complexity of monotonic alignment search (MAS) in Glow-TT is $\mathcal{O}(T_{text} \times T_{mel})$ (Kim et al., 2020), the time complexity of self-attention in VAENAR-TTS is $\mathcal{O}(1)$ (Vaswani et al., 2017), and the time complexity of auto-regressive TTS model (i.e., Tacotron2 (Shen et al.,

2018a)) is $\mathcal{O}(T_{mel})$.

For the MCD, even though BDPVAE-TTS obtains a higher MCD than VAENAR-TTS, BDPVAE-TTS captures *discrete monotonic aligned paths* in its latent space on training and inference phase which ensures model’s train and test consistency and improves model’s interpretability. VAENAR-TTS compresses the learned feature of spectrograms with conditions into Gaussian latent variables and uses these in its decoder for reconstruction. During the decoding process, these latent variables are used alongside phonemes to reconstruct the outputs. In contrast, the latent variables in BDPVAE-TTS are designed to capture phoneme-duration dependencies. This focus provides the decoder with a nuanced understanding of how the phoneme contributes to the overall speech utterance, which can be interpreted by the inference fundamental frequency (F0) in Figure 3. We provide detailed additional interpretations in Appendix H.

6.3. Application: End-to-end Singing Voice Synthesis

We extend the BDP-VAE with MA for end-to-end SVS on the popcs dataset (Liu et al., 2022). We perform this experiment not to compare with other models as in Section 6.2, but to demonstrate the utility of our method in a related task. In SVS, the longer phoneme duration also provides an opportunity to visualize the monotonically aligned optimal path clearly. The popcs contains 117 Chinese Mandarin pop songs (5 hours) collected from a qualified female vocalist. We randomly split 50 clips for inference and the rest for training. During the inference phase, the conditional inputs are the fundamental frequency and lyrics of the song clips.

Similar to TTS task, SVS task also involves unobserved structural dependencies. BDP-VAE framework could help the SVS task to capture the discrete structural dependencies in parallel, leading to an end to end framework and a better model interpretability.

Two inference results are visualized in Figure 4 where red rectangles indicate that the temporal structure between the generated Mel-spectrogram and ground truth is almost identical. As expected, the decoder of BDP-VAE synthesizes spectrograms according to the extended conditions (i.e., the phonemes) mapping by the dependency of the latent monotonic path from the prior encoder. Thus the decoder

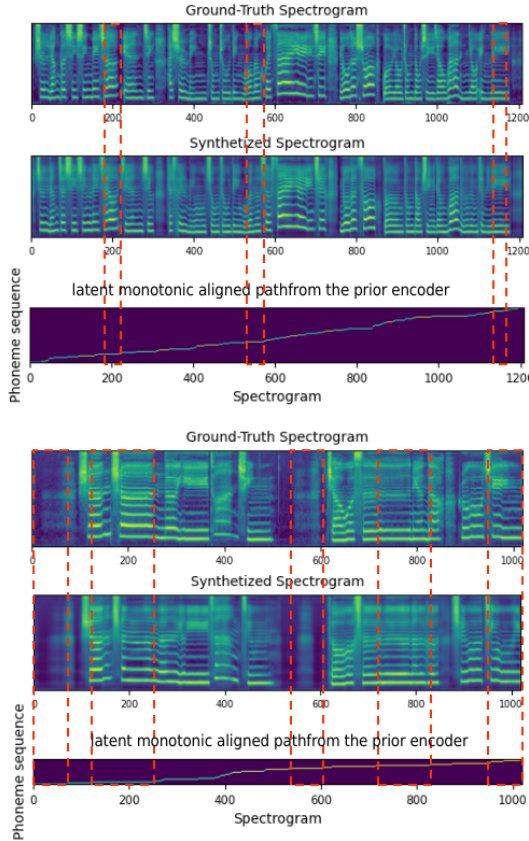


Figure 4: Visualization of GT, synthesized singing voice spectrogram, and latent optimal path from the prior encoder. *The GT and generated spectrogram are almost identical, and the generated spectrogram has a similar temporal structure to the inferred latent optimal path.*

synthesizes singing voice according to latent path-aligned phoneme conditions.

6.4. Verify Behaviour of Latent Optimal Path in BDP-VAE

To verify the behaviour and generalization of the latent optimal paths in BDP-VAE, we obtain latent optimal paths under the computational graph of DTW on the TIMIT speech corpus dataset (Garofolo et al., 1992) which includes manually time-aligned phonetic and word transcriptions. TIMIT contains English speech of 630 speakers which utterances are recorded as 16-bit 16kHz speech waveform files. We randomly split 50 clips for testing and 580 clips for training.

To the best of our knowledge, there are no existing similar works that enable VAEs to obtain hard latent optimal paths given any defined DAG structures. Thus, inspired by the experimental designs in Mensch & Blondel (2018) and Van Den Oord et al. (2017), we set the a latent distribution $\mathcal{D}(\mathcal{R}_{\text{DTW}}, \mathbf{W} = \{w \in \mathbf{W} \sim U(0, 1)\}, 1)$ as the baseline

Table 2: Mean absolute error and standard deviation (MAE/MAE \pm STD) of phoneme duration on TIMIT.

Model	Distribution	Train	Inference
BDP-VAE	$\mathcal{D}(\mathcal{R}_{\text{DTW}}, \text{NN}_{\{\phi/\theta\}}, 1)$	2.92	3.93 ± 0.37
Baseline	$\mathcal{D}(\mathcal{R}_{\text{DTW}}, \mathbf{W}_{U(0,1)}, 1)$	5.67	5.69 ± 0.31

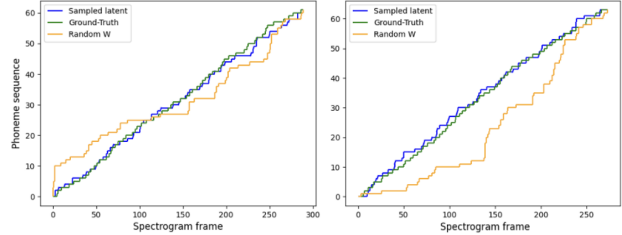


Figure 5: Visualization of GT alignment between phoneme tokens and spectrogram frames, latent optimal paths from the encoder, optimal paths from random latent space for two audio clips. *BDP-VAE achieves closer alignments with GT, indicating its effectiveness in finding latent optimal paths.*

due to lack of direct comparison. The random baseline still follows the DTW constraint with uniform edge weights, which can verify the behaviour of latent space in BPD-VAE.

We take a summation along the spectrogram dimension to obtain phoneme duration and compute the mean absolute error (MAE) between the ground truth and the phoneme duration. We input phoneme tokens and spectrogram lengths as conditions on inference to obtain latent optimal paths of the prior encoder. We repeat the inference 5 times and take the average and standard deviation of MAEs as our metric of evaluation. As in Table 2, our MAE is lower than the baseline indicating that the BDP-VAE captures meaningful information to obtain stochastic optimal paths in the latent space and is not merely guessing randomly. Figure 5 visualizes ground-truth alignments, latent optimal paths from BDP-VAE, and optimal paths from the baseline latent distribution on two audio clips, which clearly shows the latent optimal path from BDP-VAE under DTW gets a close alignment to the GT. This indicates BDP-VAE has the ability to learn informative edge weights \mathbf{W} and capture sparse optimal paths in latent space.

6.5. Sensitivity of Hyper-parameter in BDP-VAE

To study the sensitivity of the temperature parameter α , we extend the experiment in Section 6.4. Table 3 shows the MAE value on the training and inference phase with different α settings. As discussed in Section 6.1, the α affects the sharpness of the path distribution. When α is smaller, the distribution is more stochastic. As α increases, the distribution becomes sharper. However, when the α value becomes large, the latent path alignment performance

Table 3: Mean absolute error and standard deviation (MAE / MAE \pm STD) for the duration on TIMIT with different hyper-parameter α Settings.

Model	Alpha	Train	Inference
BDP-VAE	0.5	2.99	4.40 \pm 0.46
BDP-VAE	1	2.92	3.93 \pm 0.37
BDP-VAE	1.5	2.94	3.89 \pm 0.35
BDP-VAE	2	3.01	4.08 \pm 0.27
BDP-VAE	3	3.25	4.53 \pm 0.10

decreases, which is consistent with the contribution of temperature in Platt (2000). In BDP-VAE, the model with too large α may not capture enough variety of data, conversely, for too small α the model becomes too spread out and lacks meaningful structure, with the distribution approaching uniform as $\alpha \rightarrow 0$. In real applications, the value of α in BDP-VAE should be located in a reasonable range which could be found by tuning or setting a learnable parameter.

7. Conclusion

We introduce a probabilistic softening solution to the classical optimal path problem on DAGs, as stochastic optimal paths. To achieve variational Bayesian inference with latent paths, we give efficient and tractable algorithms for likelihood and KL divergence within the family of path distributions in linear time with respect to edge numbers by dynamic programming with properties of the Gumbel distribution as message-passing, namely Bayesian dynamic programming with Gumbel propagation. We demonstrate the usage of stochastic optimal paths in the VAE framework by proposing BDP-VAE. BDP-VAE captures sparse optimal paths as latent representations given a DAG and further achieves end-to-end training for generative tasks that rely on unobserved structural relationships. We showed how the BDP finds latent optimal paths under general small DAGs and demonstrated the BDP-VAE with the computational graph of monotonic alignment on two real-world applications to achieve an end-to-end framework. We verified the behaviour and generalization of the latent optimal paths under the computational graph of dynamic time warping. We also studied the sensitivity of the hyper-parameter α and gave suggestions for real applications. Our experiments show the success of our approach on generative tasks where it achieves end-to-end training involving unobserved sparse structural optimal paths. Beyond VAE, the BDP can potentially be integrated into other probabilistic frameworks or planning in model-based reinforcement learning to obtain latent paths that leave for future extensions.

Limitations and Broader Impacts: As a discrete latent variable model, BDP-VAE uses the REINFORCE estimator which may lead to high gradient variance and slow convergence during training. This limitation may be solved by involving variance reduction techniques during training.

This paper presents work whose goal is to advance the field of Machine Learning and applications of its downstream tasks. There are many potential societal consequences of our work, however, we do not foresee our methods bringing negative social impacts.

References

- Amos, B. and Kolter, J. Z. Optnet: Differentiable optimization as a layer in neural networks. In Precup, D. and Teh, Y. W. (eds.), *Proceedings of the 34th International Conference on Machine Learning, ICML 2017, Sydney, NSW, Australia, 6-11 August 2017*, volume 70 of *Proceedings of Machine Learning Research*, pp. 136–145. PMLR, 2017. URL <http://proceedings.mlr.press/v70/amos17a.html>.
- BakIr, G., Hofmann, T., Smola, A. J., Schölkopf, B., and Taskar, B. *Predicting structured data*. MIT press, 2007.
- Cai, X., Xu, T., Yi, J., Huang, J., and Rajasekaran, S. Dtw-net: a dynamic time warping network. *Advances in neural information processing systems*, 32, 2019.
- Chen, Q., Tan, M., Qi, Y., Zhou, J., Li, Y., and Wu, Q. V2C: visual voice cloning. In *IEEE/CVF Conference on Computer Vision and Pattern Recognition, CVPR 2022, New Orleans, LA, USA, June 18-24, 2022*, pp. 21210–21219. IEEE, 2022. doi: 10.1109/CVPR52688.2022.02056. URL <https://doi.org/10.1109/CVPR52688.2022.02056>.
- Chiu, C. and Raffel, C. Monotonic chunkwise attention. In *6th International Conference on Learning Representations, ICLR 2018, Vancouver, BC, Canada, April 30 - May 3, 2018, Conference Track Proceedings*. OpenReview.net, 2018. URL <https://openreview.net/forum?id=Hko85plCW>.
- Deng, Y., Kim, Y., Chiu, J. T., Guo, D., and Rush, A. M. Latent alignment and variational attention. In Bengio, S., Wallach, H. M., Larochelle, H., Grauman, K., Cesa-Bianchi, N., and Garnett, R. (eds.), *Advances in Neural Information Processing Systems 31: Annual Conference on Neural Information Processing Systems 2018, NeurIPS 2018, December 3-8, 2018, Montréal, Canada*, pp. 9735–9747, 2018. URL <https://proceedings.neurips.cc/paper/2018/hash/b691334ccf10d4ab144d672f7783c8a3-Abstract.html>.
- Djolonga, J. and Krause, A. Differentiable learning of submodular functions. In Guyon, I., von Luxburg, U., Bengio, S., Wallach, H. M., Fergus, R., Vishwanathan, S. V. N., and Garnett, R. (eds.), *Advances in Neural Information Processing Systems 30: Annual Conference*

- on *Neural Information Processing Systems 2017, December 4-9, 2017, Long Beach, CA, USA*, pp. 1013–1023, 2017. URL <https://proceedings.neurips.cc/paper/2017/hash/192fc044e74dffea144f9ac5dc9f3395-Abstract.html>.
- Garofolo, J., Lamel, L., Fisher, W., Fiscus, J., Pallett, D., Dahlgren, N., and Zue, V. Timit acoustic-phonetic continuous speech corpus. *Linguistic Data Consortium*, 11 1992.
- Halperin, T., Ephrat, A., and Peleg, S. Dynamic temporal alignment of speech to lips. In *ICASSP 2019-2019 IEEE International Conference on Acoustics, Speech and Signal Processing (ICASSP)*, pp. 3980–3984. IEEE, 2019.
- Hasegawa-Johnson, M., Cole, J., Hirschberg, J., Jilka, M., and Tannenbaum, R. Penn phonetics toolkit (p2tk): A software suite for sound analysis as a function of time. Technical report, Department of Linguistics, University of Pennsylvania, 2005.
- Heckerman, D. A tutorial on learning with bayesian networks. In Jordan, M. I. (ed.), *Learning in Graphical Models*, volume 89 of *NATO ASI Series*, pp. 301–354. Springer Netherlands, 1998. doi: 10.1007/978-94-011-5014-9_11. URL https://doi.org/10.1007/978-94-011-5014-9_11.
- Jang, E., Gu, S., and Poole, B. Categorical reparameterization with gumbel-softmax. In *5th International Conference on Learning Representations, ICLR 2017, Toulon, France, April 24-26, 2017, Conference Track Proceedings*. OpenReview.net, 2017. URL <https://openreview.net/forum?id=rkE3y85ee>.
- Jeong, M., Kim, H., Cheon, S. J., Choi, B. J., and Kim, N. S. Diff-tts: A denoising diffusion model for text-to-speech. In Hermansky, H., Cernocký, H., Burgert, L., Lamel, L., Scharenborg, O., and Motlíček, P. (eds.), *Interspeech 2021, 22nd Annual Conference of the International Speech Communication Association, Brno, Czechia, 30 August - 3 September 2021*, pp. 3605–3609. ISCA, 2021. doi: 10.21437/Interspeech.2021-469. URL <https://doi.org/10.21437/Interspeech.2021-469>.
- Kim, J., Kim, S., Kong, J., and Yoon, S. Glow-tts: A generative flow for text-to-speech via monotonic alignment search. *Advances in Neural Information Processing Systems*, 33:8067–8077, 2020.
- Kingma, D. P. and Dhariwal, P. Glow: Generative flow with invertible 1x1 convolutions. *Advances in neural information processing systems*, 31, 2018.
- Kingma, D. P. and Welling, M. Auto-encoding variational bayes. In Bengio, Y. and LeCun, Y. (eds.), *2nd International Conference on Learning Representations, ICLR 2014, Banff, AB, Canada, April 14-16, 2014, Conference Track Proceedings*, 2014. URL <http://arxiv.org/abs/1312.6114>.
- Kubichek, R. Mel-cepstral distance measure for objective speech quality assessment. In *Proceedings of IEEE pacific rim conference on communications computers and signal processing*, volume 1, pp. 125–128. IEEE, 1993.
- Li, B., Zhao, Y., Zhelun, S., and Sheng, L. Danceformer: Music conditioned 3d dance generation with parametric motion transformer. In *Proceedings of the AAAI Conference on Artificial Intelligence*, pp. 1272–1279, 2022.
- Li, N., Liu, S., Liu, Y., Zhao, S., Liu, M., and Zhou, M. Close to human quality TTS with transformer. *CoRR*, abs/1809.08895, 2018. URL <http://arxiv.org/abs/1809.08895>.
- Liu, J., Li, C., Ren, Y., Chen, F., and Zhao, Z. Diffsinger: Singing voice synthesis via shallow diffusion mechanism. In *Proceedings of the AAAI Conference on Artificial Intelligence*, pp. 11020–11028, 2022.
- Lu, H., Wu, Z., Wu, X., Li, X., Kang, S., Liu, X., and Meng, H. Vaenar-tts: Variational auto-encoder based non-autoregressive text-to-speech synthesis. *arXiv preprint arXiv:2107.03298*, 2021.
- Ma, X., Zhou, C., Li, X., Neubig, G., and Hovy, E. FlowSeq: Non-autoregressive conditional sequence generation with generative flow. In *Proceedings of the 2019 Conference on Empirical Methods in Natural Language Processing and the 9th International Joint Conference on Natural Language Processing (EMNLP-IJCNLP)*, pp. 4282–4292, Hong Kong, China, November 2019. Association for Computational Linguistics. doi: 10.18653/v1/D19-1437. URL <https://aclanthology.org/D19-1437>.
- Maddison, C. J., Tarlow, D., and Minka, T. A* sampling. *Advances in neural information processing systems*, 27, 2014.
- Maddison, C. J., Mnih, A., and Teh, Y. W. The concrete distribution: A continuous relaxation of discrete random variables. In *5th International Conference on Learning Representations, ICLR 2017, Toulon, France, April 24-26, 2017, Conference Track Proceedings*. OpenReview.net, 2017. URL <https://openreview.net/forum?id=S1jE5L5g1>.
- McAuliffe, M., Socolof, M., Mihuc, S., Wagner, M., and Sonderegger, M. Montreal forced aligner: Trainable text-speech alignment using kald. In Lacerda, F. (ed.), *Interspeech 2017, 18th Annual Conference of the International*

- Speech Communication Association, Stockholm, Sweden, August 20-24, 2017, pp. 498–502. ISCA, 2017. URL http://www.isca-speech.org/archive/Interspeech_2017/abstracts/1386.html.
- Mehrish, A., Majumder, N., Bharadwaj, R., Mihalcea, R., and Poria, S. A review of deep learning techniques for speech processing. *Information Fusion*, pp. 101869, 2023.
- Mensch, A. and Blondel, M. Differentiable dynamic programming for structured prediction and attention. In *International Conference on Machine Learning*, pp. 3462–3471. PMLR, 2018.
- Mohamed, S., Rosca, M., Figurnov, M., and Mnih, A. Monte carlo gradient estimation in machine learning. *J. Mach. Learn. Res.*, 21(132):1–62, 2020.
- Peng, K., Ping, W., Song, Z., and Zhao, K. Non-autoregressive neural text-to-speech. In *International conference on machine learning*, pp. 7586–7598. PMLR, 2020.
- Petrov, S. and Klein, D. Discriminative log-linear grammars with latent variables. In Platt, J. C., Koller, D., Singer, Y., and Roweis, S. T. (eds.), *Advances in Neural Information Processing Systems 20, Proceedings of the Twenty-First Annual Conference on Neural Information Processing Systems, Vancouver, British Columbia, Canada, December 3-6, 2007*, pp. 1153–1160. Curran Associates, Inc., 2007. URL <https://proceedings.neurips.cc/paper/2007/hash/9cc138f8dc04cbf16240daa92d8d50e2-Abstract.html>.
- Platt, J. Probabilistic outputs for support vector machines and comparison to regularized likelihood methods. In *Advances in Large Margin Classifiers*, 2000.
- Popov, V., Vovk, I., Gogoryan, V., Sadekova, T., and Kudinov, M. Grad-tts: A diffusion probabilistic model for text-to-speech. In *International Conference on Machine Learning*, pp. 8599–8608. PMLR, 2021.
- Rabiner, L. R. A tutorial on hidden markov models and selected applications in speech recognition. *Proc. IEEE*, 77(2):257–286, 1989. doi: 10.1109/5.18626. URL <https://doi.org/10.1109/5.18626>.
- Ren, Y., Ruan, Y., Tan, X., Qin, T., Zhao, S., Zhao, Z., and Liu, T.-Y. Fastspeech: Fast, robust and controllable text to speech. *Advances in Neural Information Processing Systems*, 32, 2019.
- Ren, Y., Hu, C., Tan, X., Qin, T., Zhao, S., Zhao, Z., and Liu, T.-Y. Fastspeech 2: Fast and high-quality end-to-end text to speech. *arXiv preprint arXiv:2006.04558*, 2020.
- Sakoe, H. and Chiba, S. Dynamic programming algorithm optimization for spoken word recognition. *IEEE transactions on acoustics, speech, and signal processing*, 26(1): 43–49, 1978.
- Shen, J., Pang, R., Weiss, R. J., Schuster, M., Jaitly, N., Yang, Z., Chen, Z., Zhang, Y., Wang, Y., Ryan, R., Saurous, R. A., Agiomyrgiannakis, Y., and Wu, Y. Natural TTS synthesis by conditioning wavenet on MEL spectrogram predictions. In *2018 IEEE International Conference on Acoustics, Speech and Signal Processing, ICASSP 2018, Calgary, AB, Canada, April 15-20, 2018*, pp. 4779–4783. IEEE, 2018a. doi: 10.1109/ICASSP.2018.8461368. URL <https://doi.org/10.1109/ICASSP.2018.8461368>.
- Shen, J., Pang, R., Weiss, R. J., Schuster, M., Jaitly, N., Yang, Z., Chen, Z., Zhang, Y., Wang, Y., Skerrv-Ryan, R., et al. Natural tts synthesis by conditioning wavenet on mel spectrogram predictions. In *2018 IEEE international conference on acoustics, speech and signal processing (ICASSP)*, pp. 4779–4783. IEEE, 2018b.
- Struminsky, K., Gadetsky, A., Rakitin, D., Karpushkin, D., and Vetrov, D. P. Leveraging recursive gumbel-max trick for approximate inference in combinatorial spaces. In Ranzato, M., Beygelzimer, A., Dauphin, Y. N., Liang, P., and Vaughan, J. W. (eds.), *Advances in Neural Information Processing Systems 34: Annual Conference on Neural Information Processing Systems 2021, NeurIPS 2021, December 6-14, 2021, virtual*, pp. 10999–11011, 2021. URL <https://proceedings.neurips.cc/paper/2021/hash/5b658d2a925565f0755e035597f8d22f-Abstract.html>.
- Tralie, C. and Dempsey, E. Exact, parallelizable dynamic time warping alignment with linear memory. *arXiv preprint arXiv:2008.02734*, 2020.
- Van Den Oord, A., Vinyals, O., et al. Neural discrete representation learning. *Advances in neural information processing systems*, 30, 2017.
- Vaswani, A., Shazeer, N., Parmar, N., Uszkoreit, J., Jones, L., Gomez, A. N., Kaiser, Ł., and Polosukhin, I. Attention is all you need. *Advances in neural information processing systems*, 30, 2017.
- Verdu, S. and Poor, H. V. Abstract dynamic programming models under commutativity conditions. *SIAM Journal on Control and Optimization*, 25(4):990–1006, 1987.
- Yu, L., Blunsom, P., Dyer, C., Grefenstette, E., and Kocisky, T. The neural noisy channel. *arXiv preprint arXiv:1611.02554*, 2016a.

Yu, L., Buys, J., and Blunsom, P. Online segment to segment neural transduction. *arXiv preprint arXiv:1609.08194*, 2016b.

Zandie, R., Mahoor, M. H., Madsen, J., and Emamian, E. S. Ryanspeech: A corpus for conversational text-to-speech synthesis. *ISCA*, 2021. doi: 10.21437/Interspeech.2021-341. URL <https://doi.org/10.21437/Interspeech.2021-341>.

A. Proofs of each lemma in Gumbel propagation

A.1. Proofs for Lemma 4.2

Proof. The result follows directly from (6) and (5). \square

A.2. Proofs for Lemma 4.3

Proof. The result follows directly from (6) and (5). \square

A.3. Proofs for Lemma 4.4

Proof. From the DAG structure of \mathcal{R} we have

$$\mathcal{Y}(1, v) = \bigcup_{u \in \mathcal{P}(v)} \{\mathbf{y} \cdot v : \forall \mathbf{y} \in \mathcal{Y}(1, u)\}, \quad (35)$$

where $\mathbf{y} \cdot v = (y_1, y_2, \dots, y_{|\mathbf{y}|}, v)$ denotes concatenation.

Then we have

$$\mu_v = \log \sum_{\mathbf{y} \in \mathcal{Y}(1, v)} \exp(\alpha \|\mathbf{y}\|_{\mathbf{w}}) \quad (36)$$

$$= \log \sum_{\mathbf{y} \in \bigcup_{u \in \mathcal{P}(v)} \{\hat{\mathbf{y}} \cdot v : \forall \hat{\mathbf{y}} \in \mathcal{Y}(1, u)\}} \exp(\alpha \|\mathbf{y}\|_{\mathbf{w}}) \quad (37)$$

$$= \log \sum_{u \in \mathcal{P}(v)} \sum_{\hat{\mathbf{y}} \in \mathcal{Y}(1, u)} \exp(\alpha \|\hat{\mathbf{y}} \cdot v\|_{\mathbf{w}}) \quad (38)$$

$$= \log \sum_{u \in \mathcal{P}(v)} \sum_{\hat{\mathbf{y}} \in \mathcal{Y}(1, u)} \exp(\alpha \|\hat{\mathbf{y}}\|_{\mathbf{w}} + \alpha w_{u, v}) \quad (39)$$

$$= \log \sum_{u \in \mathcal{P}(v)} \exp\left(\log \sum_{\hat{\mathbf{y}} \in \mathcal{Y}(1, u)} \exp(\alpha \|\hat{\mathbf{y}}\|_{\mathbf{w}}) + \alpha w_{u, v}\right) \quad (40)$$

$$= \log \sum_{u \in \mathcal{P}(v)} \exp(\mu_u + \alpha w_{u, v}), \quad (41)$$

where Equation (40) follows from the identity

$$\sum_i \exp(a + b_i) = \exp(a + \log \sum_i \exp(b_i)), \quad (42)$$

Equation (41) follows from

$$\mu_v = \log \sum_{\mathbf{y} \in \mathcal{Y}(1, v)} \exp(\alpha \|\mathbf{y}\|_{\mathbf{w}}) \quad (43)$$

yielding Equation (17) as required. \square

B. Proofs of each lemma in Sampling and Likelihood

B.1. Proofs for Lemma 4.5

Proof. Assuming without loss of generality that $v = N$,

$$\pi_{u,v} = p(y_{i-1} = u | y_i = v, u \in \mathcal{P}(v)) \quad (44)$$

$$= \frac{p(y_{i-1} = u, y_i = v | u \in \mathcal{P}(v))}{p(y_i = v)} \quad (45)$$

$$= \frac{1}{p(y_i = v)} \sum_{\tilde{\mathbf{y}} \in \mathcal{Y}(1,u)} p(Y = \tilde{\mathbf{y}} \cdot v) \quad (46)$$

$$= \frac{1}{p(y_i = v)} \sum_{\tilde{\mathbf{y}} \in \mathcal{Y}(1,u)} \frac{\exp(\alpha \|\tilde{\mathbf{y}} \cdot v\|_{\mathbf{W}})}{\sum_{\hat{\mathbf{y}} \in \mathcal{Y}(1,N)} \exp(\alpha \|\hat{\mathbf{y}}\|_{\mathbf{W}})} \quad (47)$$

$$\propto \sum_{\tilde{\mathbf{y}} \in \mathcal{Y}(1,u)} \exp(\alpha \|\tilde{\mathbf{y}}\|_{\mathbf{W}} + \alpha w_{u,v}) \quad (48)$$

$$\propto \exp\left(\log \sum_{\tilde{\mathbf{y}} \in \mathcal{Y}(1,u)} \exp(\alpha \|\tilde{\mathbf{y}}\|_{\mathbf{W}}) + \alpha w_{u,v}\right) \quad (49)$$

$$\propto \exp(\mu_u + \alpha w_{u,v}) \quad (50)$$

$$= \frac{\exp(\mu_u + \alpha w_{u,v})}{\sum_{\tilde{u} \in \mathcal{P}(v)} \exp(\mu_{\tilde{u}} + \alpha w_{\tilde{u},v})} \quad (51)$$

$$= \frac{\exp(\mu_u + \alpha w_{u,v})}{\exp(\mu_v)}, \quad (52)$$

where Equation (45) rewrite (44) by the rule of conditional probability, Equation (46) marginalises over $\mathbf{y}_{<i-1}$, Equation (47) extend the probability by Equation (9), Equation (48) neglects factors that do not depend on u , Equation (49) uses the identity of (42) then get Equation (50) according to Equation (15). Equation (51) makes the normalization explicit and Equation (52) uses (17) to recover Equation (19) as required. \square

C. Proofs of each lemma in KL Divergence

C.1. Proofs for Lemma 4.9

Proof. From the DAG structure of \mathcal{R} we have, for all edges $(u, v) \in \mathcal{E}$,

$$\mathcal{Y}(1, v) = \bigcup_{\mathbf{l} \in \mathcal{Y}(1, u)} \bigcup_{\mathbf{r} \in \mathcal{Y}(v, N)} \mathbf{l} \cdot \mathbf{r}, \quad (53)$$

where we recall $\mathbf{l} \cdot \mathbf{r}$ denotes concatenation. We therefore have

$$\omega_{u,v} = \sum_{\{\mathbf{y} \in \mathcal{Y}(1, N) : (u, v) \in \mathbf{y}\}} \mathcal{D}(\mathbf{y} | \mathcal{R}, \mathbf{W}, \alpha) \quad (54)$$

$$= \sum_{\{\mathbf{y} \in \mathcal{Y}(1, N) : (u, v) \in \mathbf{y}\}} \prod_{(u', v') \in \mathbf{y}} \pi_{u', v'} \quad (55)$$

$$= \sum_{\mathbf{l} \in \mathcal{Y}(1, u)} \sum_{\mathbf{r} \in \mathcal{Y}(v, N)} \prod_{(u', v') \in \mathbf{l} \cdot \mathbf{r}} \pi_{u', v'} \quad (56)$$

$$= \sum_{\mathbf{l} \in \mathcal{Y}(1, u)} \sum_{\mathbf{r} \in \mathcal{Y}(v, N)} \pi_{u,v} \prod_{(u', v') \in \mathbf{l}} \pi_{u', v'} \prod_{(u', v') \in \mathbf{r}} \pi_{u', v'} \quad (57)$$

$$= \pi_{u,v} \underbrace{\sum_{\mathbf{l} \in \mathcal{Y}(1, u)} \prod_{(u', v') \in \mathbf{l}} \pi_{u', v'}}_{\equiv \lambda_u} \underbrace{\sum_{\mathbf{r} \in \mathcal{Y}(v, N)} \prod_{(u', v') \in \mathbf{r}} \pi_{u', v'}}_{\equiv \rho_v}, \quad (58)$$

where (54) restates (21), (55) uses the chain rule of probability using Equation (20), (56) follows from (53), (57) re-factors the product and the final (58) rearranges sums and products.

Finally, it is straightforward to show by induction that the λ_u and ρ_v defined in (58) above obey the classic sum-of-product recursions given in the statement of the lemma. For example,

$$\lambda_v = \sum_{u \in \mathcal{P}(v)} \pi_{u,v} \lambda_u, \quad (59)$$

$$= \sum_{u \in \mathcal{P}(v)} \pi_{u,v} \sum_{\mathbf{l} \in \mathcal{Y}(1,u)} \prod_{(u',v') \in \mathbf{l}} \pi_{u',v'} \quad (60)$$

$$= \sum_{u \in \mathcal{P}(v)} \sum_{\mathbf{l} \in \mathcal{Y}(1,u)} \prod_{(u',v') \in \mathbf{l}} \pi_{u',v'} \quad (61)$$

$$= \sum_{\mathbf{l} \in \mathcal{Y}(1,v)} \prod_{(u,v) \in \mathbf{l}} \pi_{u,v}, \quad (62)$$

as required. □

C.2. Proofs for Lemma 4.10

Proof. We have

$$\mathcal{D}_{\text{KL}} \left[\mathcal{D}(\mathcal{R}, \mathbf{W}, \alpha) \parallel \mathcal{D}(\mathcal{R}, \mathbf{W}^{(r)}, \alpha) \right] \quad (63)$$

$$= \mathbb{E}_{\mathbf{y} \sim \mathcal{D}(\mathcal{R}, \mathbf{W}, \alpha)} \left[\log \mathcal{D}(\mathbf{y} | \mathcal{R}, \mathbf{W}, \alpha) - \log \mathcal{D}(\mathbf{y} | \mathcal{R}, \mathbf{W}^{(r)}, \alpha) \right] \quad (64)$$

$$\begin{aligned} &= \mathbb{E}_{\mathbf{y} \sim \mathcal{D}(\mathcal{R}, \mathbf{W}, \alpha)} \left[\log \frac{\exp(\alpha \|\mathbf{y}\|_{\mathbf{W}})}{\sum_{\hat{\mathbf{y}} \in \mathcal{Y}(1,N)} \exp(\alpha \|\hat{\mathbf{y}}\|_{\mathbf{W}})} \right. \\ &\quad \left. - \log \frac{\exp(\alpha \|\mathbf{y}\|_{\mathbf{W}^{(r)}})}{\sum_{\hat{\mathbf{y}} \in \mathcal{Y}(1,N)} \exp(\alpha \|\hat{\mathbf{y}}\|_{\mathbf{W}^{(r)}})} \right] \\ &= \mathbb{E}_{\mathbf{y} \sim \mathcal{D}(\mathcal{R}, \mathbf{W}, \alpha)} \left[\alpha \|\mathbf{y}\|_{\mathbf{W}} - \alpha \|\mathbf{y}\|_{\mathbf{W}^{(r)}} + \right. \end{aligned} \quad (65)$$

$$\left. \log \sum_{\hat{\mathbf{y}} \in \mathcal{Y}(1,N)} \exp(\alpha \|\hat{\mathbf{y}}\|_{\mathbf{W}^{(r)}}) - \log \sum_{\hat{\mathbf{y}} \in \mathcal{Y}(1,N)} \exp(\alpha \|\hat{\mathbf{y}}\|_{\mathbf{W}}) \right]. \quad (66)$$

The third and fourth terms inside the final expectation (on line (66)) are easily handled; *e.g.* for the third term we have

$$\begin{aligned} &\mathbb{E}_{\mathbf{y} \sim \mathcal{D}(\mathcal{R}, \mathbf{W}, \alpha)} \left[\log \sum_{\hat{\mathbf{y}} \in \mathcal{Y}(1,N)} \exp(\alpha \|\hat{\mathbf{y}}\|_{\mathbf{W}^{(r)}}) \right] \\ &= \log \sum_{\hat{\mathbf{y}} \in \mathcal{Y}(1,N)} \exp(\alpha \|\hat{\mathbf{y}}\|_{\mathbf{W}^{(r)}}) \end{aligned} \quad (67)$$

$$= \mu_N^{(r)}. \quad (68)$$

by the definition (15).

The first two terms inside the final expectation mentioned above (on line (65)) may also be efficiently re-factored; *e.g.* for the second term,

$$\begin{aligned}
 & \mathbb{E}_{\mathbf{y} \sim \mathcal{D}(\mathcal{R}, \mathbf{W}, \alpha)} [\|\mathbf{y}\|_{\mathbf{W}^{(r)}}] \\
 &= \sum_{\mathbf{y} \in \mathcal{Y}(1, N)} \mathcal{D}(\mathbf{y} | \mathcal{R}, \mathbf{W}, \alpha) \sum_{(u, v) \in \mathbf{y}} w_{u, v}^{(r)} \\
 &= \sum_{\mathbf{y} \in \mathcal{Y}(1, N)} \prod_{(u, v) \in \mathbf{y}} \pi_{u, v} \sum_{(u, v) \in \mathbf{y}} w_{u, v}^{(r)} \\
 &= \sum_{(u, v) \in \mathcal{E}} w_{u, v}^{(r)} \underbrace{\sum_{\{\mathbf{y} \in \mathcal{Y}(1, N) : (u, v) \in \mathbf{y}\}} \prod_{(u', v') \in \mathbf{y}} \pi_{u', v'}}_{\equiv \omega_{u, v}}.
 \end{aligned}$$

The expectation of (65)-(66) may therefore be rewritten as (27). \square

D. Gumbel Softmax Trick

In this section, we investigate a possible interpretation of achieving reparameterization trick (i.e., Gumbel softmax trick) on BDP-VAE framework for interested readers. Compared to the log-derivative trick discussed in Section 5.3, Gumbel softmax trick samples soft latent optimal paths and has advantages on gradient-based optimization. However, this method may require extra effort in designing its implementation and temperature parameter τ .

D.1. Node-wise Gumbel Softmax Propagation

Recall that the *Gumbel argmax* reparameterisation for the categorical distribution employs parameter-independent Gumbels via

$$\forall i \in \{1, 2, \dots, m\}, G_i \sim \mathcal{G}(0) \quad (69)$$

$$k = \operatorname{argmax}_{i \in \{1, 2, \dots, m\}} \log \mu_i + G_i, \quad (70)$$

which is equivalent to

$$k \sim \text{Categorical}(\beta_1, \beta_2, \dots, \beta_m), \quad (71)$$

where the probability β_k is equal to the r.h.s. of (7).

The *Gumbel softmax* is a differentiable approximation to the above, where the $k \in \{1, 2, \dots, m\}$ of (70) is replaced by $\kappa \in \mathbb{R}^m$ given by

$$\kappa_k = \frac{\exp((\log \mu_k + G_k)/\tau)}{\sum_{i=1}^m \exp((\log \mu_i + G_i)/\tau)}, \quad (72)$$

where τ is a free parameter. This approximation is useful for gradient-based optimization because it is both differentiable and parameterised.

Due to the generally intractable size $|\mathcal{Y}(1, N)|$ of the set of paths that make up the domain of $\mathcal{D}(\mathbf{y} | \mathcal{R}, \mathbf{W}, \alpha)$, there is no simple analogue of the above for our setting. Instead, we offer two alternative approaches, both of which are differentiable reparameterisations of a distribution of real values, one per node.

D.1.1. MARGINAL NODE-WISE GUMBEL SOFTMAX DISTRIBUTION

Consider the following

Definition D.1. Let $\mathbf{y} \sim \mathcal{D}(\mathcal{R}, \mathbf{W}, \alpha)$. The hitting probability for node v is the probability that \mathbf{y} includes v ,

$$\zeta_v \equiv p(v \in \mathbf{y}). \quad (73)$$

The node-hitting probabilities may be efficiently obtained via

Lemma D.2. *The ζ_u obey the recursion*

$$\zeta_N = 1 \tag{74}$$

$$\zeta_u = \sum_{v \in \mathcal{C}(u)} \zeta_v \pi_{u,v}, \tag{75}$$

for all $v \in \{N-1, N-2, \dots, 1\}$ (in reverse topological order w.r.t. \mathcal{R}).

We may now simply associate with each node $u \in \mathcal{V}$ a Bernoulli random variable with probability parameter ζ_u , along with a Gumbel-softmax approximation of that Bernoulli — see [subsection D.3](#) for details.

D.1.2. PATH-DEPENDENT NODE-WISE GUMBEL SOFTMAX DISTRIBUTION

Alternatively, we can soften the path sampling algorithm of [Corollary 4.7](#) to obtain a distribution over $\{\gamma_u \in [0, 1]\}_{u \in \mathcal{V}}$ that better captures the dependence between the events $u \in \mathbf{y}$ for all $u \in \mathcal{V}$. That is, we let

$$\gamma_N = 1 \tag{76}$$

$$\gamma_u = \sum_{v \in \mathcal{C}(u)} \gamma_v \delta_{u,v}, \tag{77}$$

for all $u \in \{N-1, N-2, \dots, 1\}$ (in reverse topological order w.r.t. \mathcal{R}), where $\delta_{u,v}$ is the Gumbel-softmax analog to step 2 of [Corollary 4.7](#), namely

$$\forall (u, v) \in \mathcal{E}, G_{u,v} \sim \mathcal{G}(0) \tag{78}$$

$$\delta_{u,v} = \frac{\exp((\log \pi_{u,v} + G_{u,v})/\tau)}{\sum_{i \in \mathcal{C}(u)} \exp((\log \pi_{u,i} + G_{u,i})/\tau)}. \tag{79}$$

D.2. KL Divergence Between two Gumbels

Lemma D.3. *The KL divergence between unit variance Gumbels is*

$$\mathcal{D}_{\text{KL}} [\mathcal{G}(\alpha) \parallel \mathcal{G}(\beta)] = \alpha - \beta + (1 - \exp(\alpha - \beta)) \text{Ei}(-\exp(-\alpha)), \tag{80}$$

in terms of the standard special “exponential integral” function

$$\text{Ei}(z) \equiv - \int_{-z}^{\infty} \exp(-t)/t \, dt. \tag{81}$$

Proof.

$$\begin{aligned} & \mathcal{D}_{\text{KL}} [\mathcal{G}(\alpha) \parallel \mathcal{G}(\beta)] \\ &= \int_0^{\infty} G(x|\alpha) \log \frac{G(x|\alpha)}{G(x|\beta)} \, dx \\ &= \int_0^{\infty} \exp(-(x-\alpha) - \exp(x-\alpha)) \log \frac{\exp(-(x-\alpha) - \exp(x-\alpha))}{\exp(-(x-\beta) - \exp(x-\beta))} \, dx \\ &= \int_0^{\infty} \exp(-(x-\alpha) - \exp(x-\alpha)) (\alpha - \beta + \exp(x-\beta) - \exp(x-\alpha)) \, dx \\ &= \alpha - \beta + I_1 - I_2 \\ &= \alpha - \beta + (1 - \exp(\alpha - \beta)) \text{Ei}(-\exp(-\alpha)), \end{aligned}$$

because

$$\begin{aligned} I_2 &\equiv \int_0^{\infty} \exp(-\exp(x-\alpha)) \, dx \\ &= -\text{Ei}(-\exp(-\alpha)) \end{aligned}$$

and

$$\begin{aligned} I_1 &\equiv \int_0^\infty \exp(\alpha - \beta - \exp(x - \alpha)) dx \\ &= -\exp(\alpha - \beta) \text{Ei}(-\exp(-\alpha)), \end{aligned}$$

giving the desired result. \square

D.3. Binary Gumbel (Soft) Max

For the binary case, we can sample just one logistic random variable, rather than two Gumbels, as per the traditional Gumbel max trick. Let $X \sim \text{Bernoulli}(\zeta)$. The Gumbel max parameterised, for $g_1, g_2 \sim \mathcal{G}(0)$

$$X = \underset{k \in \{1,2\}}{\text{argmax}} (\log \zeta + g_1, \log(1 - \zeta) + g_2)_k \quad (82)$$

$$= \underset{k \in \{1,2\}}{\text{argmax}} (\log \zeta, \log(1 - \zeta) + l)_g \quad (83)$$

where we may show that $l = g_2 - g_1 \sim \text{Logistic}(0, 1)$.² The soft-max analogue $X_\tau \in (0, 1)$ of X , where τ is a temperature parameter, is therefore

$$X_\tau \equiv \frac{\exp(\tau^{-1} \log \zeta)}{\exp(\tau^{-1} \log \zeta) + \exp(\tau^{-1} (\log(1 - \zeta) + l))}. \quad (84)$$

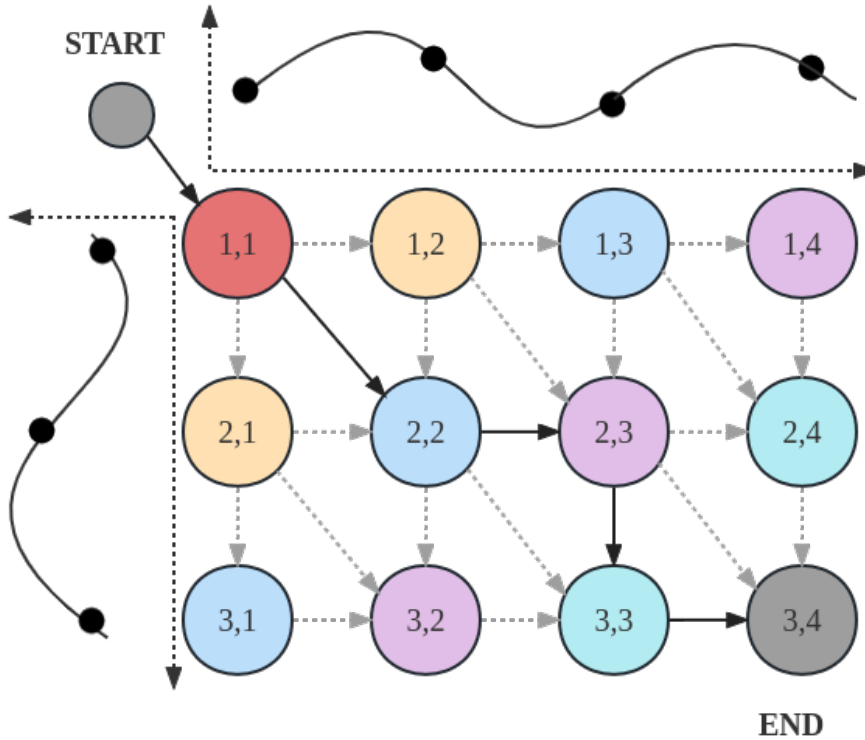


Figure 6: Computational graph \mathcal{R} of the DTW algorithm

E. Examples of computational graphs

We demonstrate two examples of how to implement the *Bayesian dynamic programming* to obtain structural latent optimal paths on different structured computational graphs.

²https://en.wikipedia.org/wiki/Logistic_distribution

Algorithm 1 Compute μ and π on DTW

Input: Weight matrix $\mathbf{W} \in \mathbb{R}^{N_B \times N_A}$, α ;
 Initialize $\mu \in \mathbb{R}^{(N_B+1) \times (N_A+1)}$,
 $\mu_{i,0} = -\infty, \mu_{0,j} = -\infty, i \in [N_B], j \in [N_A]$;
 $\mu_{0,0} = 0$;
for $i = 1$ **to** $N_B, j = 1$ **to** N_A **do**
 $\mu_{i,j} = \log(\exp(\mu_{i-1,j-1} + \alpha w_{i,j}) + \exp(\mu_{i,j-1} + \alpha w_{i,j}) + \exp(\mu_{i-1,j} + \alpha w_{i,j}))$
end for
 Initialize $\pi_{i,j} = \mathbf{0}_3, i \in [N_B], j \in [N_A]$;
for $i = N_B$ **to** $1, j = N_A$ **to** 1 **do**
 $\pi_{i,j} = \left[\frac{\exp(\mu_{i,j-1} + \alpha w_{i,j})}{\exp(\mu_{i,j})}, \frac{\exp(\mu_{i-1,j-1} + \alpha w_{i,j})}{\exp(\mu_{i,j})}, \right.$
 $\left. \frac{\exp(\mu_{i-1,j} + \alpha w_{i,j})}{\exp(\mu_{i,j})} \right]$
end for

E.1. Dynamic Time Warping

We first extend the Bayesian dynamic programming on the dynamic time warping (DTW) algorithm (Sakoe & Chiba, 1978; Mensch & Blondel, 2018) which aims to seek an optimal alignment path with the maximum score (or minimum cost) given two time series. Given two time-series \mathbf{A} and \mathbf{B} with lengths N_A and N_B . Let a_j and b_i be the j^{th} and i^{th} observations of \mathbf{A} and \mathbf{B} , respectively. We denote $\mathbf{W} \in \mathbb{R}^{N_B \times N_A}$ as a pair-wise weight matrix, where w_{ij} represents similarity measurement between observation point b_i and observation point a_j , namely, $w_{ij} = d(b_i, a_j)$, where function $d(\cdot)$ is an arbitrary similarity metric. The \mathcal{Y} defines the set of the population of all possible time-series alignment paths \mathbf{y} , in which the path connects the upper-left $(1, 1)$ node to the lower-right (N_B, N_A) node with \rightarrow, \downarrow and \searrow moves only.

Following Lemma 4.4, we can obtain the location parameters $\mu \in \mathbb{R}^{N_B \times N_A}$ given the DAG \mathcal{R} and \mathbf{W} . Then the optimal path \mathbf{y} can be sampled reversely according to the transition matrix $\pi \in \mathbb{R}^{N_B \times N_A \times 3}$. The probability of transition $(v, v') \rightarrow (u, u')$, where $(u, u') \in \mathcal{P}(v, v')$, is defined as

$$\pi_{(u,u'),(v,v')} \equiv p(y_{i-1} = (u, u') | y_i = (v, v'), (u, u') \in \mathcal{P}(v, v')) \quad (85)$$

for all $i \in \{(1, 1), \dots, (N_B, N_A)\}$

Figure 6 is an example of the computational graph of DTW with $N_A = 4$ and $N_B = 3$. The bold black arrows indicate one aligned path $\mathbf{y} \in \mathcal{Y}$ on the DAG. Pseudocode to compute the location parameter μ and transition matrix π and sampling optimal path \mathbf{y} are provided in Algorithm 1 and Algorithm 2.

We denote the marginal probability of edges between node (u, u') and node (v, v') , where $(u, u') \in \mathcal{P}(v, v')$, as $\omega_{(u,u')(v,v')}$. Following Lemma 4.9, the ω can be computed by Equation (86)

$$\omega_{(u,u'),(v,v')} = \pi_{(u,u'),(v,v')} \lambda_{(u,u')} \rho_{(v,v')} \quad (86)$$

For implementation, the pseudocode to compute the marginal probabilities ω show on Algorithm 3.

E.1.1. TIME COMPLEXITY ANALYSIS

Following above definition of the computational graph of DTW, where the pair-wise weight matrix $\mathbf{W} \in \mathbb{R}^{N_B \times N_A}$. According to Corollary 4.11, the edge numbers under DTW graph is $|\mathcal{E}| = 3N_A N_B - 2N_A - 2N_B + 1$. Therefore, the time complexity in above pseudo algorithm is $\mathcal{O}(3N_A N_B - 2N_A - 2N_B + 1)$. Inspired by Tralie & Dempsey (2020), we further reduce its time complexity by updating diagonally in parallel as illustrated in Figure 7. In this way, the time complexity of computational graph of DTW becomes linear N_B and N_A as $\mathcal{O}(N_A + N_B - 1)$.

E.2. Monotonic Alignment

Monotonic alignment (MA) is often used in the field of machine learning, particularly in the context of sequence-to-sequence (Seq2Seq) models. Taking the same definition of two given time-series in Appendix E.1, \mathcal{Y} defines a population of all

Algorithm 2 Sample alignment path y on DTW

Input: Transition matrix $\pi \in \mathbb{R}^{N_B \times N_A \times 3}$
 Initialize $y \in \mathbb{R}^{N_B \times N_A}$, $i = N_B$, $j = N_A$;
 $y_{N_B, N_A} = 1$, $y_{N_B, / N_A} = 0$;
while $i > 0$ and $j > 0$ **do**
 $x \sim \text{Categorical}(\pi_{i,j})$
 if $x = 0$ **then**
 $y_{i,j-1} = 1$
 $j = j - 1$
 end if
 if $x = 1$ **then**
 $y_{i-1,j-1} = 1$
 $i = i - 1$
 $j = j - 1$
 end if
 if $x = 2$ **then**
 $y_{i-1,j} = 1$
 $i = i - 1$
 end if
end while

possible path sample \mathbf{y} , in which the path connects the upper-left $(1, 1)$ node to the lower-right (N_B, N_A) node with \rightarrow and \searrow moves only, where $N_B < N_A$.

The location parameters $\mu \in \mathbb{R}^{N_B \times N_A}$ can be computed following the Lemma 4.4 and the optimal path \mathbf{y} can be sampled according to the transition matrix $\pi \in \mathbb{R}^{N_B \times N_A \times 2}$. The probability of transition $(v, v') \rightarrow (u, u')$ for $(u, u') \in \mathcal{P}(v, v')$ is defined in Equation (85). Figure 8 gives an example of the monotonic alignment computational graph with $N_A = 7$ and $N_B = 4$. The bold black arrows indicate one possible aligned path.

Pseudocode of computing the location parameter μ and transition matrix π are provided in Algorithm 4. The sampling algorithm is presented in Algorithm 5.

We then denote the marginal probability of edges between node (u, u') and node (v, v') , where $(u, u') \in \mathcal{P}(v, v')$, as $\omega_{(u,u'),(v,v')}$. The ω can be computed by Equation (86) and the pseudocode to compute the marginal probabilities ω show on Algorithm 6.

E.2.1. TIME COMPLEXITY ANALYSIS

Following the setting of computational graph of MA in above, where the pair-wise weight matrix $\mathbf{W} \in \mathbb{R}^{N_B \times N_A}$ and the graph is defined in Figure 8, where $N_B < N_A$. The edge number under MA graph is $|\mathcal{E}| = N_B N_A - N_B^2$ and the time complexity in pseudo algorithms of computational graph of MA is $\mathcal{O}(N_B N_A - N_B^2)$. By updating the graph vertically as illustrated in Figure 9, the time complexity can be further reduced to $\mathcal{O}(N_A - 1)$.

F. Details of model architecture in experiments

Given a spectrogram input $\mathbf{x} = [x_1, \dots, x_t]$ and a corresponding phoneme text $\mathbf{c}' = [c'_1, \dots, c'_n]$, where t and n are the lengths of the input sequences. We assume that there is an unobserved alignment representation $\mathbf{y} \in \mathbb{R}^{t \times n}$ aligns \mathbf{x} and \mathbf{c} by $\{0, 1\}$ only.

The proposed overall architecture is shown in Figure 10 and the conditional ELBO is

$$\begin{aligned}
 \mathcal{L}(\phi, \theta, \mathbf{x} | \mathbf{c}) &= \mathbb{E}_{\mathbf{y} \sim q(\cdot | \mathbf{x}, \mathbf{c}; \phi)} [\log p(\mathbf{x} | \mathbf{y}, \mathbf{c}; \theta)] \\
 &\quad - \mathcal{D}_{\text{KL}} [q(\mathbf{y} | \mathbf{x}, \mathbf{c}; \phi) \| p(\mathbf{y} | \mathbf{c}; \theta)].
 \end{aligned} \tag{87}$$

Algorithm 3 Compute marginal probability of edges ω on DTW

Input: Transition matrix $\pi \in \mathbb{R}^{N_B \times N_A \times 3}$
 Initialize $\omega \in \mathbb{R}^{N_B \times N_A \times 3}$; $\omega_{i,j} = 0$; $i \in [N_B], j \in [N_A]$
 $\lambda, \rho \in \mathbb{R}^{(N_B+1) \times (N_A+1)}$;
 $\lambda_{i,j} = 0$; $i \in [N_B], j \in [N_A]$; $\lambda_{0,0} = 1$;
 $\rho_{i,j} = 0$, $i \in [N_B], j \in [N_A]$; $\rho_{N_B, N_A} = 1$;
 {Topological iteration for λ }
for $i = 1$ **to** N_B , $j = 1$ **to** N_A **do**
 $\lambda_{i,j} = [\lambda_{i,j-1}, \lambda_{i-1,j-1}, \lambda_{i-1,j}] \pi_{i,j}^T$
end for
 {Reversed iteration for ρ }
for $i = N_B$ **to** 1 , $j = N_A$ **to** 1 **do**
 $\rho_{i,j} = [\rho_{i,j+1}, \rho_{i+1,j+1}, \rho_{i+1,j}] [\pi_{i,j+1,0}, \pi_{i+1,j+1,1}, \pi_{i+1,j,2}]^T$
end for
 {Compute ω }
for $i = 1$ **to** N_B , $j = 1$ **to** N_A **do**
 $\omega_{i,j} = \rho_{i,j} [\lambda_{i,j-1}, \lambda_{i-1,j-1}, \lambda_{i-1,j}]^T \cdot \pi_{i,j}$
end for

Algorithm 4 Compute μ and π on MA

Input: Weight matrix $\mathbf{W} \in \mathbb{R}^{N_B \times N_A}$, α ;
 Initialize $\mu \in \mathbb{R}^{(N_B+1) \times (N_A+1)}$
 $\mu_{i,j} = -\infty$, $i \in [N_B], j \in [N_A]$; $\mu_{0,0} = 0$;
for $j = 1$ **to** N_A **do**
 for $i = 1$ **to** $\min(j, N_B)$ **do**
 $\mu_{i,j} = \log(\exp(\mu_{i-1,j-1} + \alpha w_{i,j}) + \exp(\mu_{i,j-1} + \alpha w_{i,j}))$
 end for
end for
 Initialize $\pi_{i,j} = \mathbf{0}_2$, $i \in [N_B], j \in [N_A]$;
for $j = N_A$ **to** 1 **do**
 for $i = \min(j, N_A)$ **to** $\max(j - N_A + N_B, 1)$ **do**
 $\pi_{i,j} = \left[\frac{\exp(\mu_{i,j-1} + \alpha w_{i,j})}{\exp(\mu_{i,j})}, \frac{\exp(\mu_{i-1,j-1} + \alpha w_{i,j})}{\exp(\mu_{i,j})} \right]$
 end for
end for

Text Encoder The text encoder is used to extract a higher level of linguistic feature $\mathbf{c} \in \mathbb{R}^{n \times 256}$ from phoneme text, which adopts the same structures as the one in FastSpeech2 (Ren et al., 2020), which contains 4 Feed-forward Transformer blocks with 2 multi-head attentions.

Posterior Encoder The posterior encoder $q(\mathbf{y}|\mathbf{x}, \mathbf{c}; \phi) = \mathcal{D}(\mathbf{y}|\mathcal{R}, \mathbf{W} = d(\text{NN}_\phi(\mathbf{x}), \mathbf{c}), \alpha)$, where α is a preset hyperparameter. Note that the gradient with respect to θ will not backpropagate to the text encoder. The architecture of the posterior encoder shouldn't be too complex, its goal is to extract temporal information from spectrogram inputs \mathbf{x} by a neural network model parameterized by ϕ . In the posterior encoder (Figure 11), the spectrogram is fed into a convolution-based PostNet (Shen et al., 2018b) to upsample the feature dimension to the size of the linguistic feature \mathbf{c} , i.e. $\text{NN}_\phi(\mathbf{x}) \in \mathbb{R}^{t \times 256}$. The final weight matrix $\mathbf{W} \in \mathbb{R}^{t \times n}$ computed by

$$d(f_\phi(\mathbf{x}), \mathbf{c}) = \text{softmax}(\text{NN}_\phi(\mathbf{x})\mathbf{c}^T) \quad (88)$$

where the softmax function is applied over the t dimension.

Decoder The architecture of the decoder is also the same as the one in FastSpeech2 (Ren et al., 2020). In the decoder (Figure 12), the alignment latent \mathbf{y} and the linguistic feature \mathbf{c} are extended by a matrix multiplication which extends

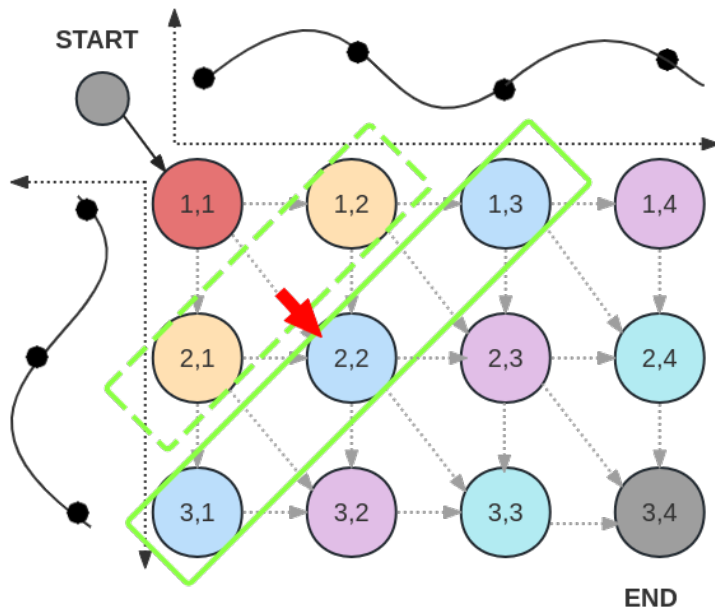


Figure 7: Updating the computational graph of DTW diagonally with linear time complexity to N_B and N_A .

the linguistic feature from length n to length t according to the alignment information, then followed by 4 Feed-forward Transformer blocks with 2 multi-head attentions. We add a residual connection after the linear layer with a PostNet to get the final output.

Prior Encoder The prior encoder $p(\mathbf{y}|\mathbf{c}; \theta) = \mathcal{D}(\mathbf{y}|\mathcal{R}, \mathbf{W}^{(0)} = d(f_\theta(\mathbf{c}), \mathbf{c}), \alpha)$. Following Lu et al. (2021); Ma et al. (2019), we make use of a Glow (Kingma & Dhariwal, 2018) structure to infer spectrogram features condition on linguistic features. It consists of multiple Glow blocks. Each of the blocks has an actnorm layer, an invertible 1×1 convolutional layer, and an affine-coupling layer. The transformation network in the affine-coupling layer is based on the Transformer decoder which the spectrogram feature $\text{NN}_\phi(\mathbf{x})$ as the query and the linguistic feature \mathbf{c} as the key and value. During training, we use the backward pass to infer the probability of the KL divergence. The forward pass is used to generate spectrogram features from the condition and then form the weight matrix to sample latent $\hat{\mathbf{y}}$ during inference. Details of the architecture are in Figure 13.

Length Predictor Following Lu et al. (2021), the length predictor consists of a 1-channel fully connected layer with ReLU activation. The length predictor is optimized by an MSE loss and the gradient will not propagate to the text encoder.

G. Experimental details

G.1. Experimental Setup

All experiments were performed on one NVIDIA GeForce RTX 3090. To reduce the variance of gradients during training, we applied the variance reduction technique with a 5-iteration moving average baseline on the REINFORCE loss. The moving average baseline technique here is used for reducing the gradient variance for the REINFORCE estimator.

G.2. Experimental Details for End-to-end Text-to-speech

In the experiment of the end-to-end text-to-speech on the computational graph of MA in Appendix E.2, the latent space captures the monotonic alignment path between phoneme tokens and spectrogram frames. We down-sampled the audio waveform files from 44.1kHz to 22.05kHz and extracted the Mel-spectrograms with 1024 frame size, 25% overlapping, and 80 filter channels. The model is trained by 18 batch size with a learning rate of $1.25e^{-4}$, temperature parameter α of 5 for

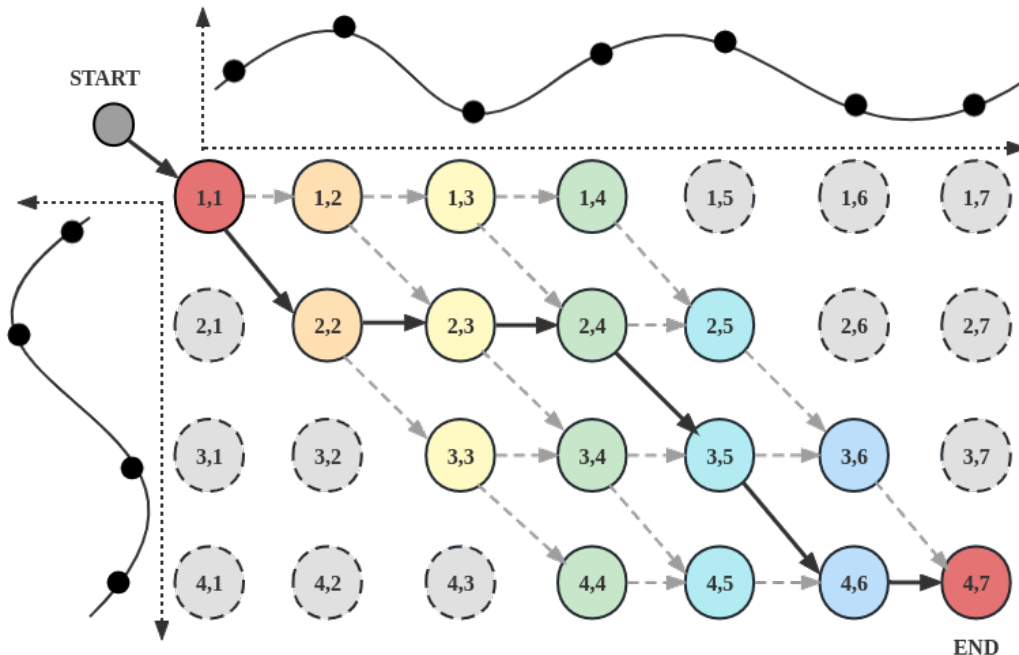


Figure 8: Computational graph \mathcal{R} of the MA algorithm.

700k steps.

In the evaluation part, we obtain the DTW-MCD score by the package of *pymcd.mcd*³. The 60-iteration Griffin-Lim Algorithm approximates all the synthesized waveforms. We trained all the models in Table 1 with the same pre-processing setting and the details are:

FastSpeech2 FastSpeech2 (Ren et al., 2020) is a non-end-to-end TTS model with additional inputs of energy, pitch, phoneme-align TextGrid from MAF⁴. We followed the model configuration the paper provided. We trained the model by 400k iterations and the total loss converged at around $6.9e^{-3}$.

Tacotron2 Tractorn2 (Shen et al., 2018a) is an end-to-end auto-regressive TTS model that relies on attention to obtain the phoneme duration alignment. We followed the model configuration provided and trained the model by 100k iterations and the total loss converged at around $6.6e^{-3}$.

VAENAR-TTS VAENAR-TTS (Lu et al., 2021) is an end-to-end utterance-level TTS model that relies on cascade attention in the decoder of the VAE to obtain the phoneme duration alignment. We followed the model configuration the paper provided and trained the model by 150k iterations and the total loss converged at around $7.4e^{-3}$.

Glow-TTS Glow-TTS (Kim et al., 2020) is an end-to-end phoneme-level TTS model that relies on the monotonic alignment search to obtain the hard phoneme duration alignment. We followed the model configuration the paper provided and trained the model by 120k iterations and the total loss converged at around -2.1 .

G.3. Experimental Details for the End-to-end Singing Voice Synthesis

In the experiment of the end-to-end singing voice synthesis on the computational graph of MA in Appendix E.2, we extract the Mel-spectrogram by the same pre-processing setting as the experiment of end-to-end TTS. The model is trained by the same architecture configuration with 22 batch sizes and a learning rate of $1.25e^{-4}$ for 200k steps. The 60-iteration Griffin-Lim Algorithm approximates all the synthesized waveforms.

³<https://github.com/chenqi008/V2C>

⁴<https://montreal-forced-aligner.readthedocs.io/en/latest/>

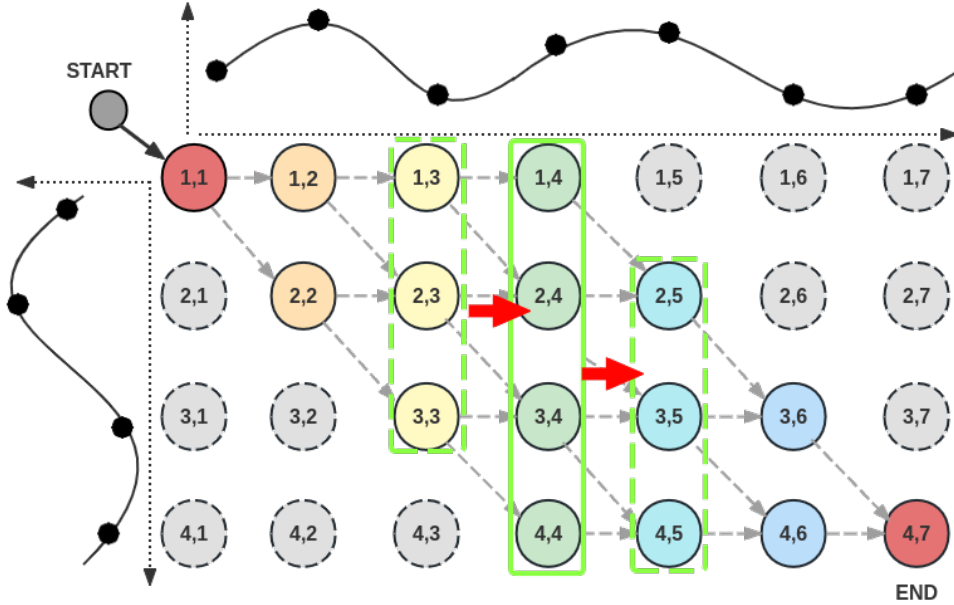


Figure 9: Updating the computational graph of MA vertically with linear time complexity to N_B and N_A .

G.4. Experimental Details for Latent optimal path on the computational graph of DTW

In the experiment of the latent optimal path on the computational graph of DTW in Appendix E.1, we use the TIMIT dataset (Garofolo et al., 1992) which is recorded by a 16kHz sampling rate. Therefore, we extract the Mel-spectrogram with 1024 frame size, 25% overlapping, and 80 filter channels under a 16kHz sampling rate. The model is trained with batch size 48 and learning rate $2.5e^{-4}$.

H. Interpretation with the comparison of VAENAR-TTS

Both BDPVAE-TTS and VAENAR-TTS predict phone-duration alignment on the utterance level. VAENAR-TTS learns the Gaussian latent distribution of learned features of spectrograms and conditions and obtains soft monotonic phoneme-utterance alignment by attention with a causality mask in VAE’s transformer decoder. Different from VAENAR-TTS, BDPVAE-TTS was adapted from a non-end-to-end phoneme-level TTS model (FastSpeech2 (Ren et al., 2020)) with a distribution of stochastic optimal paths $\mathcal{D}(\mathcal{R}, \cdot, \alpha)$ into a BDP-VAE framework. Thus, during its inference time, BDPVAE-TTS reconstructs the spectrogram according to phoneme duration aligned phoneme tokens only. Since our baseline method (i.e., FastSpeech2) did not outperform the VAENAR-TTS, thus, BDPVAE-TTS also gets a lower performance than VAENAR-TTS.

However, soft alignment in VAENAR-TTS may make the model cannot accurately capture the exact relationship of how phoneme tokens perform in a spectrogram. According to the natural inherent relationship of speech and phonemes, the BDPVAE-TTS obtains sparse monotonical optimal paths in the latent space which are more precise in explaining the relationship between utterance and phoneme tokens. Figure 14 to Figure 16 give additional demonstrations that the synthesized audios from BDPVAE-TTS have closer F0 to the ground truth than VAENAR-TTS.

Algorithm 5 Sample alignment path y on MA

Input: Transition matrix $\pi \in \mathbb{R}^{N_B \times N_A \times 2}$
Initialize $y \in \mathbb{R}^{N_B \times N_A}$, $i = N_B, j = N_A$;
 $y_{N_B, N_A} = 1, y_{/ N_B, / N_A} = 0$;
while $i > 0$ and $j > 0$ **do**
 $x \sim \text{Categorical}(\pi_{i,j})$
 if $x = 0$ **then**
 $y_{i,j-1} = 1$
 $j = j - 1$
 end if
 if $x = 1$ **then**
 $y_{i-1,j-1} = 1$
 $i = i - 1$
 $j = j - 1$
 end if
end while

Algorithm 6 Compute marginal probability of edges ω on MA

Input: Transition matrix $\pi \in \mathbb{R}^{N_B \times N_A \times 2}$
Initialize $\omega \in \mathbb{R}^{N_B \times N_A \times 2}$; $\omega_{i,j} = 0$; $i \in [N_B], j \in [N_A]$
 $\lambda, \rho \in \mathbb{R}^{(N_B+1) \times (N_A+1)}$;
 $\lambda_{i,j} = 0$; $i \in [N_B], j \in [N_A]$; $\lambda_{0,0} = 1$;
 $\rho_{i,j} = 0$, $i \in [N_B], j \in [N_A]$; $\rho_{N_B, N_A} = 1$;
{Topological iteration for λ }
for $j = 1$ **to** N_A **do**
 for $i = 1$ **to** $\min(j, N_B)$ **do**
 $\lambda_{i,j} = [\lambda_{i,j-1}, \lambda_{i-1,j-1}] \pi_{i,j}^T$
 end for
end for
{Reversed iteration for ρ }
for $j = N_A$ **to** 1 **do**
 for $i = \min(j, N_B)$ **to** $\max(j - N_A + N_B, 1)$ **do**
 $\rho_{i,j} = [\rho_{i,j+1}, \rho_{i+1,j+1}] [\pi_{i,j+1,0}, \pi_{i+1,j+1,1}]^T$
 end for
end for
{Compute ω }
for $j = 1$ **to** N_A **do**
 for $i = 1$ **to** $\min(j, N_B)$ **do**
 $\omega_{i,j} = \rho_{i,j} [\lambda_{i,j-1}, \lambda_{i-1,j-1}]^T \cdot \pi_{i,j}$
 end for
end for

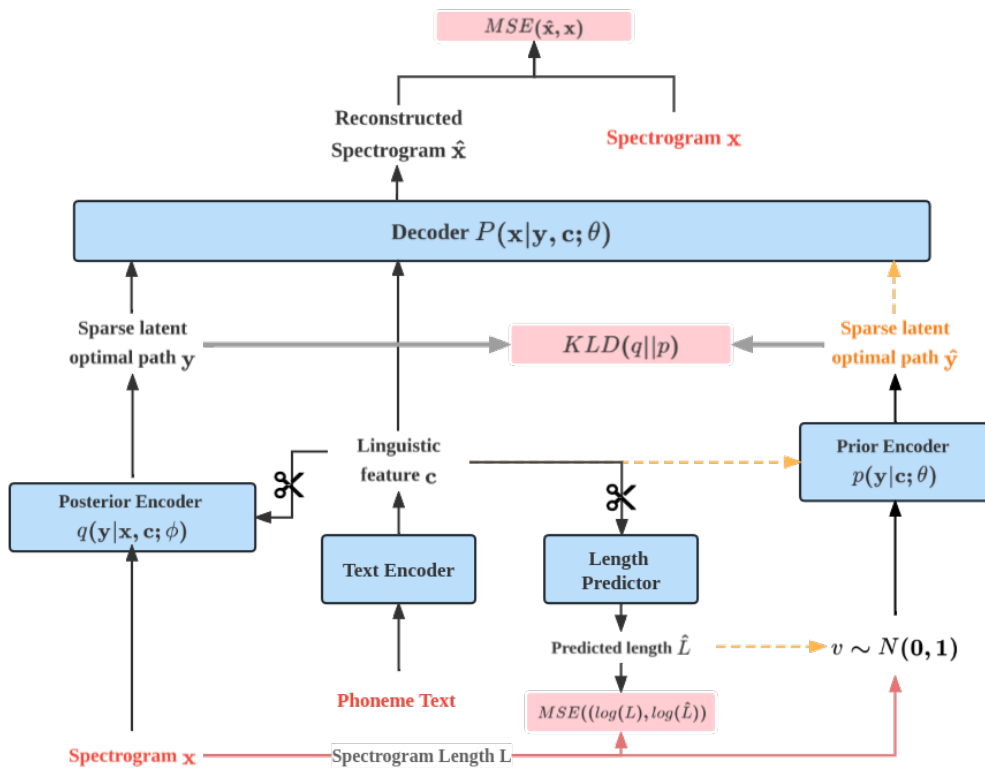


Figure 10: Architecture of BDP-VAE on experiments. The red lines are only turned on during training. Black lines stand for the training process while yellow dotted lines stand for the inference phase. The scissors represent the gradient not being back-propagated along with the arrow.

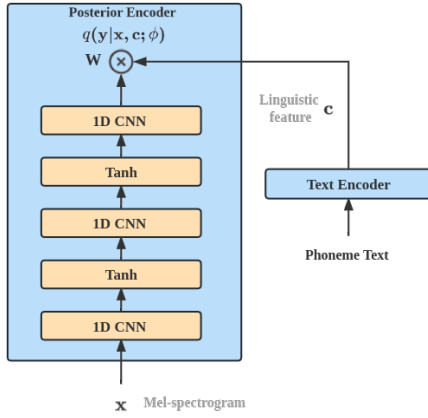


Figure 11: The posterior encoder architecture, where the \otimes represents Equation (88).

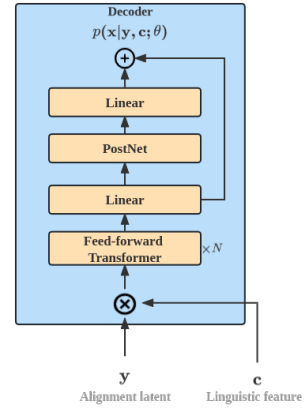


Figure 12: The decoder architecture, where the \otimes represents the matrix multiplication.

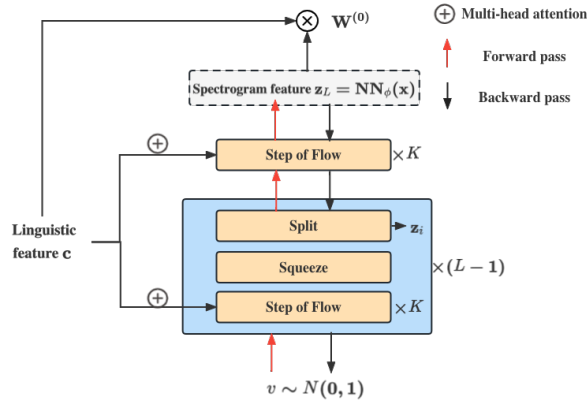


Figure 13: The conditional prior encoder architecture, where the \otimes represents Equation (88).

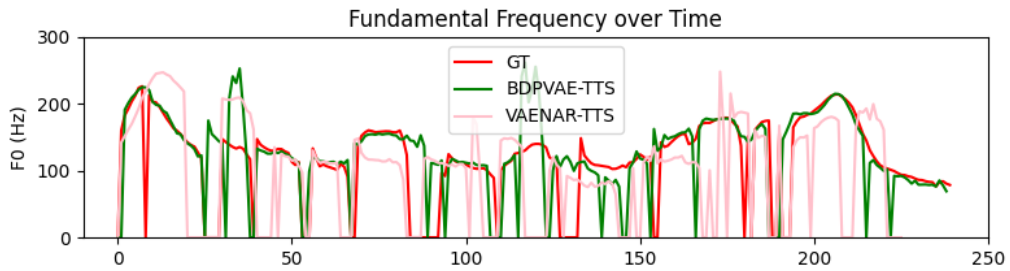


Figure 14: Inference F0 trajectories of utterance "I don't think I can talk about nature without smiling".

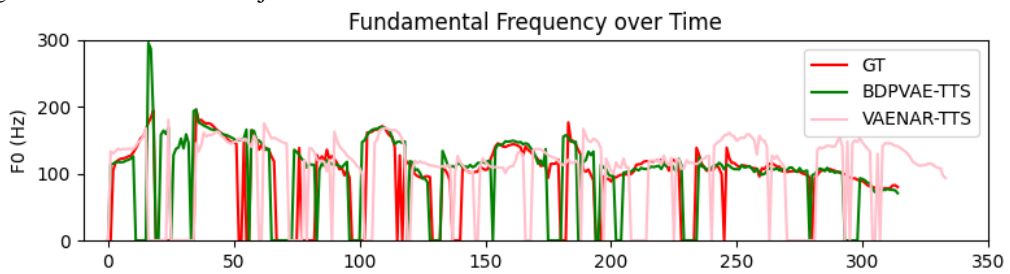


Figure 15: Inference F0 trajectories of utterance "I leaped back into the compartment of the han ship and knelt beside my wilma.".

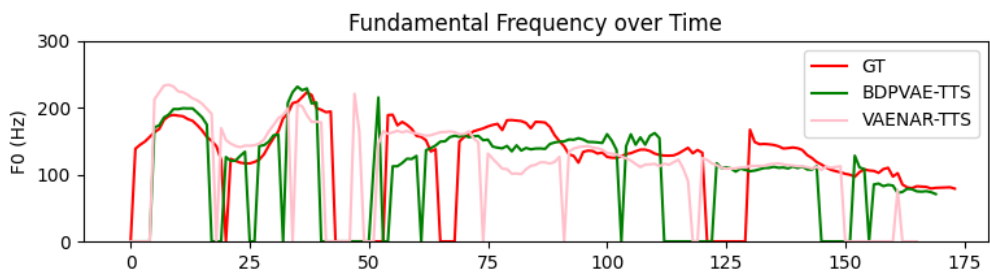


Figure 16: Inference F0 trajectories of utterance "I have reached the end of my explanation".